nature communications

Article

https://doi.org/10.1038/s41467-024-55050-y

A high-protein diet-responsive gut hormone regulates behavioral and metabolic optimization in *Drosophila melanogaster*

Received: 29 January 2024

Accepted: 27 November 2024

Published online: 30 December 2024

Check for updates

Yuto Yoshinari[1,2] ✉, Takashi Nishimura[1] ✉, Taishi Yoshii[3], Shu Kondo[4,5], Hiromu Tanimoto[6], Tomoe Kobayashi[7], Makoto Matsuyama[7] & Ryusuke Niwa[2] ✉

Protein is essential for all living organisms; however, excessive protein intake can have adverse effects, such as hyperammonemia. Although mechanisms responding to protein deficiency are well-studied, there is a significant gap in our understanding of how organisms adaptively suppress excessive protein intake. In the present study, utilizing the fruit fly, *Drosophila melanogaster*, we discover that the peptide hormone CCHamide1 (CCHa1), secreted by enteroendocrine cells in response to a high-protein diet (HPD), is vital for suppressing overconsumption of protein. Gut-derived CCHa1 is received by a small subset of enteric neurons that produce short neuropeptide F, thereby modulating protein-specific satiety. Importantly, impairment of the CCHa1-mediated gut-enteric neuronal axis results in ammonia accumulation and a shortened lifespan under HPD conditions. Collectively, our findings unravel the crosstalk of gut hormone and neuronal pathways that orchestrate physiological responses to prevent and adapt to dietary protein overload.

Protein is a macronutrient essential for all living organisms. In various species, intake of dietary protein regulates growth, metabolism, fecundity, and lifespan, and amino acid sensing is crucial for adaptation to the nutritional environment. Mechanisms by which animals respond to dietary protein restriction have been extensively studied. For example, upon protein deficiency, essential amino acids (EAAs) are key nutrients, sensed by a pathway comprising general control nonderepressible 2 (GCN2) and activating transcription factor 4 (ATF4), as well as the mechanistic target of rapamycin complex 1 (mTORC1) pathway[1]. More recently, the non-essential amino acids (NEAAs) tyrosine and cysteine have been shown to govern local and systemic adaptive responses to a low-protein diet in the fruit fly, *Drosophila melanogaster*[2,3].

On the other hand, when animals consume enough protein, they can suppress excessive protein intake through various mechanisms. In particular, high-protein diets (HPD) induce robust suppression of food intake, greater than that of an isocaloric load of fat or carbohydrates. This suppression is related to the ability of organisms to adaptively adjust their feeding behavior based on the protein content of the diet, with HPD tending to suppress food intake and low-protein diets tending to increase it[4,5]. Importantly, excessive protein intake leads to adverse effects, such as hyperammonemia[6]. However, the response mechanism when excess protein is consumed is still largely unknown compared to the responsive mechanism when protein intake is deficient.

Drosophila melanogaster, has emerged as a leading model organism to study mechanisms of nutrient-sensing and food choice,

[1]Metabolic Regulation and Genetics, Institute for Molecular and Cellular Regulation, Gunma University, Maebashi, Japan. [2]Life Science Center for Survival Dynamics, Tsukuba Advanced Research Alliance (TARA), University of Tsukuba, Tennodai 1-1-1, Tsukuba, Ibaraki 305-8577, Japan. [3]Graduate School of Environmental, Life, Natural Science and Technology, Okayama University, Okayama, Japan. [4]Department of Biological Science and Technology, Faculty of Advanced Engineering, Tokyo University of Science, Tokyo, Japan. [5]Invertebrate Genetics Laboratory, National Institute of Genetics, Mishima, Japan. [6]Graduate School of Life Sciences, Tohoku University, Sendai, Japan. [7]Division of Molecular Genetics, Shigei Medical Research Institute, Okayama, Japan. ✉e-mail: yuto.yoshinari@gunma-u.ac.jp; t-nishimura@gunma-u.ac.jp; ryusuke-niwa@tara.tsukuba.ac.jp

due to the simplicity of its neural circuitry and behavior[7–10]. *Drosophila melanogaster* makes food choices based on metabolic and physiological demands. For instance, flies that ingest food after starvation prefer sugar to protein[8]. Moreover, post-mating females with an increased need for egg production selectively consume protein-rich food[10]. Mechanisms underlying this adaptive behavior are thought to involve a sophisticated decision-making system that integrates internal and external cues to generate appropriate behavioral responses at the individual level.

In this study, using *D. melanogaster*, we present findings that shed light on mechanisms suppressing excessive protein intake to avoid hyperammonemia under HPD. Specifically, we provide evidence that the neuropeptide CCHamide1 (CCHa1), which is secreted by enteroendocrine cells (EECs), suppresses protein overload. *Drosophila melanogaster* EECs also secrete hormones in response to nutrients, such as sugars, to control feeding-related events and metabolism[11–18]. Here, we found that CCHa1-producing EECs respond positively to excessive protein. Furthermore, gut-derived CCHa1 is received by a restricted population of enteric neurons, producing short neuropeptide F (sNPF). These enteric neurons modulate nutrient-specific satiety and metabolism against HPD by communicating with the fructose receptor, Gustatory receptor 43a (Gr43a)-positive neighboring neurons. Collectively, our findings unravel the crosstalk between gut hormone and neuronal pathways that orchestrate physiological responses to prevent and adapt to dietary protein overload.

Results

Midgut CCHa1 regulates feeding behavior in female *Drosophila melanogaster*

The initial aim of this study was to examine which enteroendocrine hormones influence food intake in *D. melanogaster*. For this purpose, we knocked down each of the identified enteroendocrine hormones in adult EECs and quantified food intake for 24 h using the capillary feeder assay (CAFÉ) assay. For adult EEC-specific knockdown, we conducted transgenic RNAi using a GAL4 driver (*pros^{V1}-GAL4*) coupled with *tub-GAL80^{ts}* (hereafter *pros^{ts}-GAL4*) (Fig. 1a). In this study, we primarily focused on adult virgin females because mating induces increased food intake associated with activation of oogenesis[10,19].

Drosophila melanogaster EECs produce multiple peptide hormones, such as Allatostatin A (AstA), Allatostatin C (AstC), Bursicon α (Bursα), CCHa1, CCHamide2 (CCHa2), Diuretic hormone 31 (Dh31), Neuropeptide F (NPF), Orcokinin, and Tachykinin (Tk)[20]. Among the nine peptide hormones examined, knockdown of *CCHa1* or *AstA* resulted in a significant increase in food intake (Fig. 1b). In subsequent analyses, we decided to focus on *CCHa1* because of the pronounced phenotype of RNAi animals. The hyperphagic phenotype was also observed with the other *CCHa1* RNAi line (*CCHa1$^{RNAi\,KK}$*) that targeted a different region of *CCHa1* mRNA (Fig. 1c). We also confirmed that knockdown of *CCHa1* with *pros^{ts}-GAL4* suppresses *CCHa1* mRNA expression in a gut-specific manner (Fig. 1d, Supplementary Fig. 1a, b). These results suggest that the food intake phenotype is due to the loss of *CCHa1* function in EECs.

We further ruled out the possibility that *CCHa1* in the central nervous system (CNS), which regulates circadian behavioral rhythms[21], affects feeding behavior. Combining a transgene *otd-nls::flp* that expresses FLP recombinase only in the brain with *tub > FRT > GAL80 > FRT*, we were able to restrict *nSyb-GAL4* activity to the brain (referred to as *nSyb^{Brain}-GAL4*) (Supplementary Fig. 1c). *nSyb^{Brain}-GAL4* allowed us to suppress most *CCHa1* expression in the brain, but not in EECs (Supplementary Fig. 1c). Nevertheless, brain-specific knockdown of *CCHa1* with *nSyb^{Brain}-GAL4* did not promote feeding behavior, indicating that CCHa1 in the brain does not regulate feeding (Fig. 1c). Furthermore, we found that knocking down *CCHa1* in the posterior region (R4-5) of EECs with *R65D05-GAL4*, a *GAL4* driven by a fragment sequence upstream of *AstA*, increased food intake in a manner similar to *pros^{ts}-GAL4*-dependent *CCHa1* knockdown (Fig. 1c). Notably, *R65D05-GAL4*-mediated *CCHa1* RNAi did not affect CCHa1 protein levels in the CNS (Supplementary Fig. 1d), supporting our idea that gut-derived CCHa1 regulates feeding behavior.

Since the food used for the standard CAFÉ assay contained a mixture of sucrose and yeast autolysate, we conducted a two-choice CAFÉ assay utilizing a solution containing either sucrose or yeast autolysate. *CCHa1* RNAi animals consumed more yeast autolysate than control animals, while their sucrose intake remained unaffected (Fig. 1e), suggesting that the loss of gut-derived CCHa1 selectively impacts appetite regulation for yeast. Since yeast is a source of dietary protein for *D. melanogaster*, we also examined dietary protein intake using tryptone, a digested casein, to directly evaluate appetite against proteins. *CCHa1* RNAi animals consumed more tryptone than control animals, indicating that gut-derived CCHa1 regulates protein satiety response (Fig. 1f). A short-term feeding experiment with FlyPAD[7] for 60 min corroborated these results by demonstrating a similar trend in increased protein feeding in *CCHa1* knockdown (Fig. 1g). Thus, our findings imply that gut-derived CCHa1 is pivotal in regulating the protein satiety response in *D. melanogaster*.

Recently, it became evident that metabolic and behavioral characteristics of *D. melanogaster* exhibit sexual dimorphism[22–24]. Accordingly, we investigated whether loss of *CCHa1* in the gut impacts behavioral phenotypes in male flies. As in female flies described above, gut-specific *CCHa1* knockdown males displayed an increase in feeding compared to controls (Supplementary Fig. 1e). However, contrary to the response in females, gut-specific *CCHa1* knockdown in males did not result in a preferential shift to high-protein intake (Supplementary Fig. 1f). Therefore, these results suggest that CCHa1 in the gut regulates feeding behavior in both male and female flies, but there appears to be sexual dimorphism, at least in preference.

CCHa1-producing EECs respond to HPDs and amino acids

Recent studies on *D. melanogaster* have reported that specific nutrients have the ability to stimulate EECs, leading to secretion of enteroendocrine hormones to affect downstream target organs[11,13]. To investigate effects of protein and sugar on activity of CCHa1$^+$ EECs, we utilized the calcium reporter system, CaLexA[25], to facilitate cumulative tracing of Ca^{2+} signaling activity (Fig. 2a, b, Supplementary Fig. 2a). Compared with the standard diet (SD), a HPD, the 10% peptone-supplemented diet increased activity of CCHa1$^+$ EECs located in the posterior midgut (Supplementary Fig. 2a, c). Moreover, other protein-rich diets, such as a yeast-only diet, a 4% yeast-supplemented diet, and a 10% tryptone-supplemented diet, also increased the activity of CCHa1$^+$ EECs, whereas the glucose-only diet did not affect the activity of CCHa1$^+$ EECs (Supplementary Fig. 2b, c). This HPD-dependent activation of CCHa1$^+$ EECs is consistent with a recent study showing that HPD feeding activates CCHa1$^+$ EECs and affects arousability through CCHa1$^+$ EECs in male flies[16].

Since HPD activates CCHa1$^+$ EECs, we suspected that amino acids are critical to activating EECs. To identify these amino acids, we added several kinds of amino acid mixtures to the SD and confirmed the activity of CCHa1$^+$ EECs. We found that a mixture of all amino acids and NEAA activated CCHa1$^+$ EECs, whereas a mixture of EAA did not (Fig. 2a, b). Moreover, knocking down gut-derived *CCHa1* increased NEAA solution feeding and exhibited a preference shift toward NEAA solution (Fig. 2c, Supplementary Fig. 2d). To further determine which NEAA amino acids are crucial, we conducted experiments by setting three groups (Mix 1, 2, and 3), each of which contained only a few kinds of NEAA amino acids (see Methods). Among them, NEAA Mix3, which contained glycine (Gly), alanine (Ala), proline (Pro), and tyrosine (Tyr), activated the CCHa1$^+$ EEC (Fig. 2a, b). Adding any one of these amino acids failed to activate CCHa1$^+$ EEC; however, removing Ala from the NEAA Mix3 abolished CCHa1$^+$ EEC activation (Fig. 2d, and Supplementary Fig. 2e). These data suggest that Ala is required for activation

https://doi.org/10.1038/s41467-024-55050-y

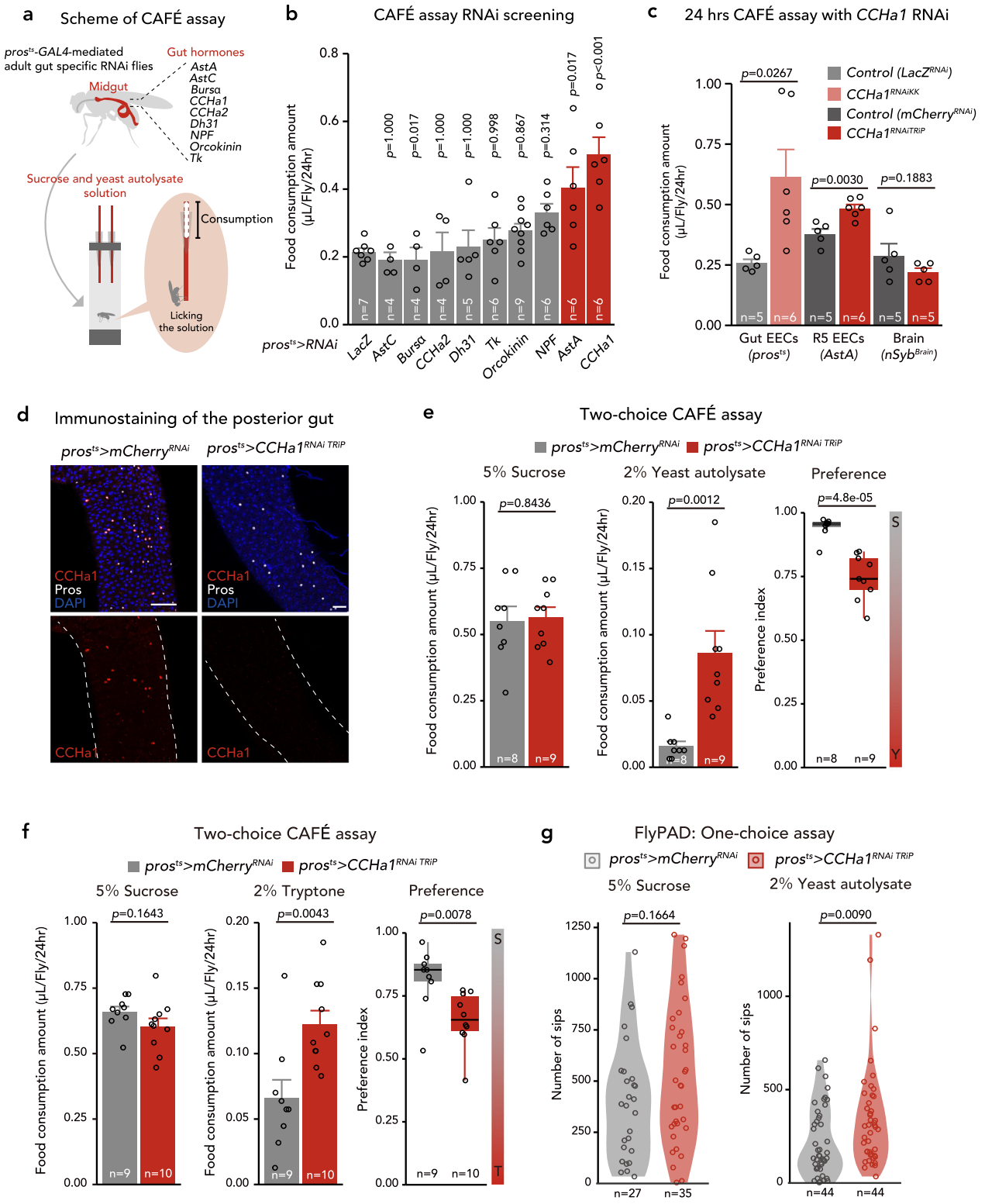

of CCHa1$^+$ EECs. Moreover, the SD supplemented with a mixture of Ala and Gly activated CCHa1$^+$ EEC, whereas the addition of Ala and Pro or of Ala and Tyr did not (Fig. 2e). On the other hand, even the addition of twice the amount of Ala did not activate CCHa1$^+$ EEC (Fig. 2e), suggesting that the combination of Ala and Gly is essential. In addition to the CaLexA signals, HPD increased *CCHa1* mRNA levels in the gut and the number of EECs immunostained with anti-CCHa1 antibodies in the posterior midgut (Supplementary Fig. 2f, g). Although CCHa1 protein levels in the gut were increased by HPD, NEAA, All AA, or NEAA Mix3-supplemented diet (Supplementary Fig. 2h), the CCHa1 protein level did not always correlate with CaLexA activity because an EAA-supplemented diet, which does not activate CCHa1$^+$ EECs, also increased the CCHa1 protein level (Fig. 2b and Supplementary Fig. 2h).

To further examine the effects of HPD or amino acid-supplemented diet on Ca^{2+} signaling, we expressed the calcium sensor GCaMP8f in CCHa1$^+$ EECs. We found fluctuating GCaMP8f signals in these cells with HPD or Ala and Gly-supplemented diet, although brightness varied among cells (Fig. 2f, g, and Supplementary Movie. 1).

Fig. 1 | Midgut CCHa1 regulates feeding behavior in female *Drosophila melanogaster*. **a** The gut and capillary feeding (CAFÉ) assay showing the experimental scheme. **b** Screening of enteroendocrine hormones, which affect feeding amount in the CAFÉ assay. **c** The CAFÉ assay with *CCHa1* RNAi in the Gut EECs (*pros*^{ts}), EECs of R5 region midgut (*AstA*), and brain (*nSyb*^{brain}). **d** Immunostaining images of the midgut from control or gut-specific *CCHa1* RNAi flies. CCHa1 (Red), Prospero (white), and DAPI (blue) are shown. In the bottom images, white broken lines show the outlines of the midgut. Scale bar, 50 μm. **e** Two-choice feeding experiment with CAFÉ assay. Consumption of sucrose (left), yeast autolysate (centre), and preference (right) of control or gut-specific *CCHa1* RNAi flies is shown. In this and the following two-choice CAFÉ assay figures, each dot presents a sample of eight flies. In the preference graph, S means sucrose, Y means yeast autolysate. **f** Two-choice feeding experiment with CAFÉ assay. Consumption of sucrose (left), tryptone (centre), and preference (right) is shown. **g** Number of sips of sucrose (left) and yeast autolysate (right) of *CCHa1* RNAi or control flies measured using the flyPAD system. In this and the following flyPAD assay figures, a dot presents the number of sips by a single fly from each food source measured separately. Numbers of samples assessed (*n*) are shown in the graphs. For all bar graphs, means and SEMs with all data points are shown. For box plots with dots, the median, 25th and 75th percentile lines are shown. Whiskers extend 1.5 times the interquartile range from the 25th and 75th percentiles. Statistics: One-way ANOVA followed by Dunnett's test (**b**), two-tailed Student's *t* test (**c**, **e**, **f**), two-sided Wilcoxon rank sum test (**g**). *p* values are shown in the graphs.

This fluctuation occurred more frequently with HPD or Ala and Gly-supplemented diet-fed flies than with SD-fed flies (Fig. 2h). Notably, only about half of the CCHa1$^+$ EECs responded to the HPD or amino acid-supplemented diet in the CaLexA and GCaMP experiments (Fig. 2f, g and Supplementary Fig. 2c). These results suggest that half of CCHa1$^+$ EECs respond to HPD or amino acid-supplemented diet and that CCHa1$^+$ EECs are heterogeneous.

To investigate whether manipulation of EEC activity leads to similar effects as *CCHa1* RNAi in the gut, we inhibited cellular activity of CCHa1$^+$ EECs by overexpressing the temperature-sensitive allele of dynamin, *shibire*^{ts}, which blocks synaptic transmission and vesicle endocytosis, specifically in CCHa1$^+$ EECs. For this purpose, we employed *R57C10-GAL80*, which inhibits GAL4 activity in neurons. By combining *CCHa1-T2A-knock-in-GAL4* with *R57C10-GAL80*, we could restrict GAL4 activity to just posterior EECs (Supplementary Fig. 3a). Using these genetic tools, we confirmed that inhibition of CCHa1$^+$ EECs by *shibire*^{ts} results in accumulation of CCHa1 protein in EECs (Supplementary Fig. 3b). Additionally, inhibiting CCHa1 secretion increased feeding amount, and promoted protein feeding, as in *CCHa1* RNAi (Supplementary Fig. 3c, d). These findings support our idea that CCHa1$^+$ EECs regulate satiety in response to dietary proteins.

Appetite for proteins is regulated by several humoral factors, including *Drosophila* insulin-like peptides (Dilps) and female-specific independent of transformer (Fit) in adult female *D. melanogaster*[8,26]. Gut-specific *CCHa1* RNAi animals showed a reduction of *dilp2, dilp5*, and *fit* mRNA expression in the head, compared to controls, whereas *dilp3* mRNA expression was increased (Supplementary Fig. 3e). These data are consistent with previous results that the reduction of *dilp2* or *fit* mRNA expression evokes a preference for protein-rich food[8,26]. In addition, expression of *dilp5*, which mRNA is reduced by starvation[27,28], was also reduced in *CCHa1* RNAi animals (Supplementary Fig. 3e). Note that *CCHa1* RNAi males did not show any effect on *fit* mRNA expression, implying that *fit* may control feeding behavior in females, but not in males (Supplementary Fig. 3f). Together, these data suggest that CCHa1 in midgut EECs suppresses protein feeding by activating them in response to excessive dietary protein.

CCHa1 receptor in sNPF neurons regulates sugar/protein feeding balance

We next explored the role of the CCHa1 receptor (CCHa1-R) in controlling protein satiety. Consistent with Fly Cell Atlas data showing enrichment of *CCHa1-R* expression in the nervous system[29], we found that *CCHa1-R-T2A-knock-in-GAL4* was predominantly expressed in the nervous system (Fig. 3a). Moreover, nervous system-specific *CCHa1-R* knockdown by pan-neuronal *GAL4* (*nSyb-GAL4*) exhibited a similar increase in feeding amount and feeding preference shift to gut-specific *CCHa1* RNAi (Fig. 3b), suggesting that CCHa1 targets the nervous system to control feeding behavior.

To identify a specific subset of *CCHa1-R*$^+$ neurons responsible for suppressing protein feeding, we took a two-choice CAFÉ assay screen with several neuronal *GAL4* drivers. Among the neuronal *GAL4* lines tested, *short NPF* (*sNPF*)*-GAL4* driver showed a significant preference shift as observed in *nSyb > CCHa1-R*^{RNAi} (Fig. 3c). Importantly, knockdown of *CCHa1-R* in cells involved in feeding preference, such as insulin-producing cells (*dilp2-GAL4*)[26] and corpora cardiaca (*Akh-GAL4*)[13], did not result in a feeding preference shift (Fig. 3c). Moreover, *CCHa1-R* RNAi in a subset of *CCHa1-R*$^+$ neurons in the mushroom body regulating sleep[16] also exhibited no effects on feeding preference (Fig. 3c). We obtained a similar preference shift with another *UAS-CCHa1-R RNAi* line (*UAS-CCHa1-R*$^{RNAi\ VDRC}$) (Fig. 3d, Supplementary Fig. 4a).

Since *sNPF-GAL4* labeled more than 100 neurons in the nervous system (Fig. 3e), we tried further restricting *sNPF* neurons. To this end, we conducted a second screen with *sNPF*-promoter *GAL4* drivers. Whereas the feeding preference against sucrose and tryptone differ between *GAL4* lines, only the *sNPF*TH*-GAL4* driver[30] induced a shift in feeding preference from sucrose to tryptone by *CCHa1-R* knockdown using two RNAi lines targeting different mRNA sequence (Fig. 3f, g). Therefore, we focused on *sNPF*TH*-GAL4*$^+$ neurons as a target of gut-derived CCHa1 to suppress protein feeding.

Two or three pairs of enteric sNPF neurons control feeding balance

We next analyzed the expression pattern of *sNPF*TH*-GAL4*. Intriguingly, the *sNPF*TH*-GAL4* driver did not label any neurons in the brain, the abdominal ganglion, or EECs in the gut, whereas it labeled two or three pairs of enteric neurons in the hypocerebral ganglion (HCG)[31,32] (Fig. 4a, b, Supplementary Fig. 5a). *sNPF*TH*-GAL4*$^+$ enteric neurons were co-labeled with anti-sNPF/NPF antibodies. Furthermore, their signals disappeared in *sNPF* knockdown and *sNPF* null mutants, indicating that they are sNPF-producing neurons (Supplementary Fig. 5b, c). Notably, enteric sNPF neurons were labeled with the *CCHa1-R-T2A-knock-in-GAL4* driver, suggesting that *CCHa1-R* is expressed in enteric neurons (Supplementary Fig. 5d). Knocking down *sNPF* in enteric neurons or *sNPF* genetic null mutants resulted in a significant feeding preference shift, similar to loss of CCHa1/CCHa1-R signaling (Fig. 4c, Supplementary Fig. 5e). Moreover, *sNPF* knockdown increased yeast autolysate intake in a short-term one-choice FlyPAD experiment (Fig. 4d). These data suggest that sNPF in *CCHa1-R*$^+$ enteric neurons is crucial in suppressing protein feeding.

Consistent with the fact that HPD activates CCHa1$^+$ EECs, we found that HPD leads to activation of enteric sNPF neurons using *sNPF*TH*-GAL4*-driven *CaLexA > GFP* flies (Fig. 4e, f). Moreover, *CCHa1-R* knockdown canceled the increase in GFP signals in the HPD-fed condition, indicating that CCHa1-R signaling is required to activate enteric sNPF neurons (Fig. 4e, f). Moreover, suppression of activity of enteric sNPF neurons by *shibire*^{ts} also showed a preference shift to protein (Fig. 4g). While CCHa1/CCHa1-R signaling and a HPD regulate neuronal activity of enteric sNPF neurons, knocking down *CCHa1* did not affect *sNPF* mRNA expression and protein levels (Supplementary Fig. 6a, b). On the other hand, HPD increases *sNPF* mRNA levels regardless of genotype (Supplementary Fig. 6a). Therefore, CCHa1 controls feeding behavior through regulation of neuronal activity rather than *sNPF* mRNA expression.

https://doi.org/10.1038/s41467-024-55050-y

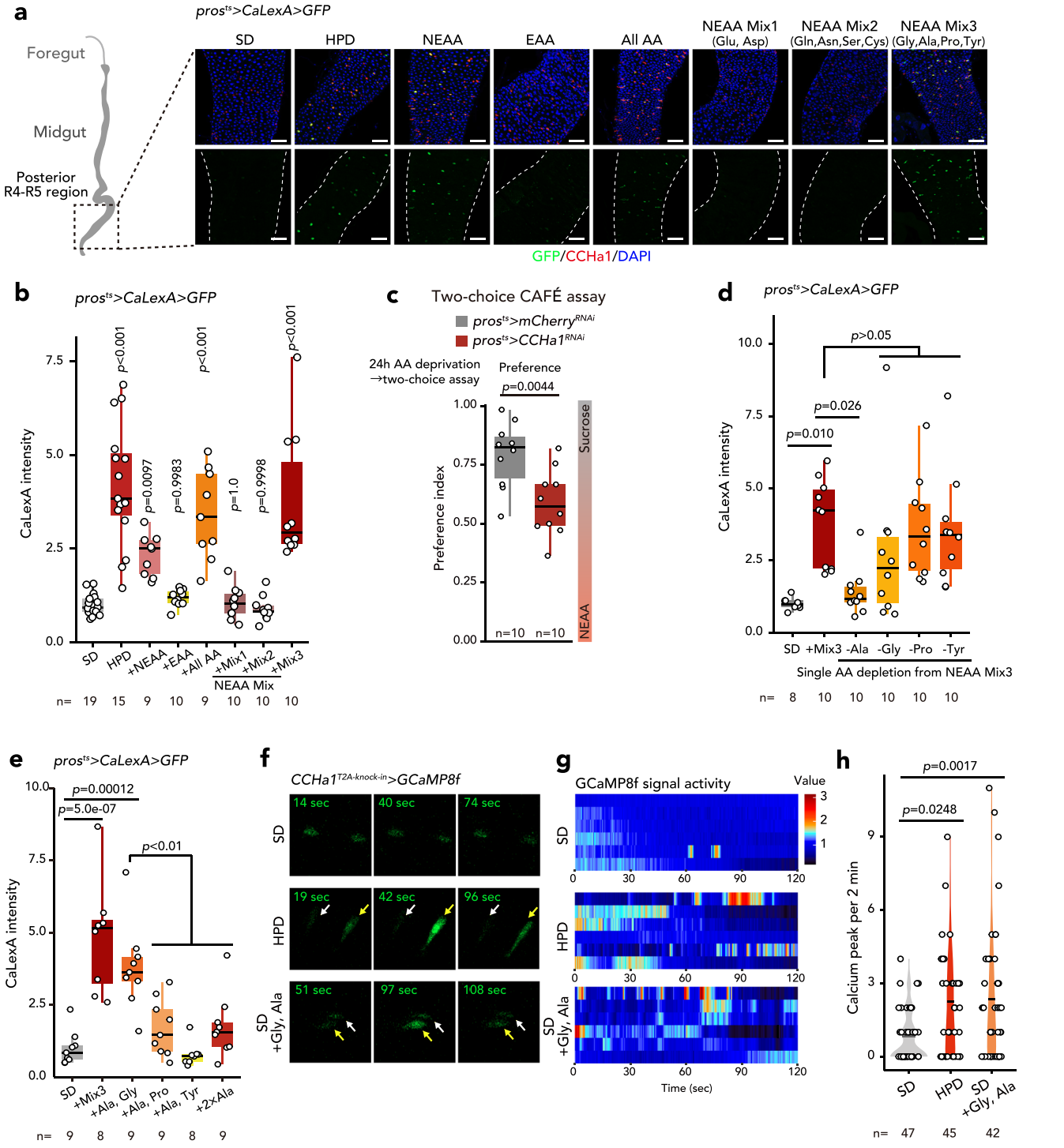

Fig. 2 | High-protein diets and amino acid-supplemented diets activate CCHa1⁺ EECs. Besides the standard diet without supplementation (SD) and HPD, other diets consisted of standard diets supplemented with NEAA, EAA, all amino acids (All AA), and selected combinations of NEAA (Mix 1, 2, and 3). Amino-acid compositions of these mixtures are described in Supplementary Data 1. **a** (Left) Illustration of the gut showing posterior region of midgut. (Right) Immunostaining images of the midgut from *pros^{ts}>CaLexA > GFP* flies expressing a Ca^{2+}-signaling-sensitive reporter in EECs maintained on each medium. GFP (green), CCHa1 (red), and DAPI (blue) are shown. White broken lines show the outline of the midgut. Scale bar, 20 μm. **b** Quantification of the GFP signal of CCHa1⁺ EECs of *pros^{ts}>CaLexA > GFP* flies maintained as in (**a**). **c** Two-choice feeding experiment with the CAFÉ assay. Preference between sucrose and the NEAA mixture of control and gut-specific *CCHa1* RNAi flies is shown. **d**, **e** Quantification of the GFP signal of CCHa1⁺ EECs of *pros^{ts}>CaLexA > GFP* flies. **f** Sequential images of *CCHa1-$^{T2A\text{-}knock\text{-}in}$-GAL4*-driven GCaMP8f signals in EECs. The timestamp indicates the time elapsed since the start of imaging. White arrows and yellow arrows indicate non-responders and responders, respectively. **g** Representative heatmap records of GCaMP8f intensity of six individual EECs from single gut. **h** Quantification of Ca^{2+} peak in EECs within 2 min under different feeding conditions. Numbers of samples assessed (*n*) are shown in the graphs. For box plots with dots, the median, 25th and 75th percentile lines are shown. Whiskers extend 1.5 times the interquartile range from the 25th and 75th percentiles. Statistics: One-way ANOVA followed by Dunnett's test (**b**), two-tailed Student's *t* test (**c**), one-way ANOVA followed by Tukey's multiple comparisons test (**d**, **e**, **h**). *p* values are shown in the graphs. The exact *p* values for Fig. 2e; +Ala, Gly vs +Ala, Pro (0.0063), +Ala, Gly vs +Ala, Tyr (0.0082), +Ala, Gly vs +2x Ala (0.000060).

https://doi.org/10.1038/s41467-024-55050-y

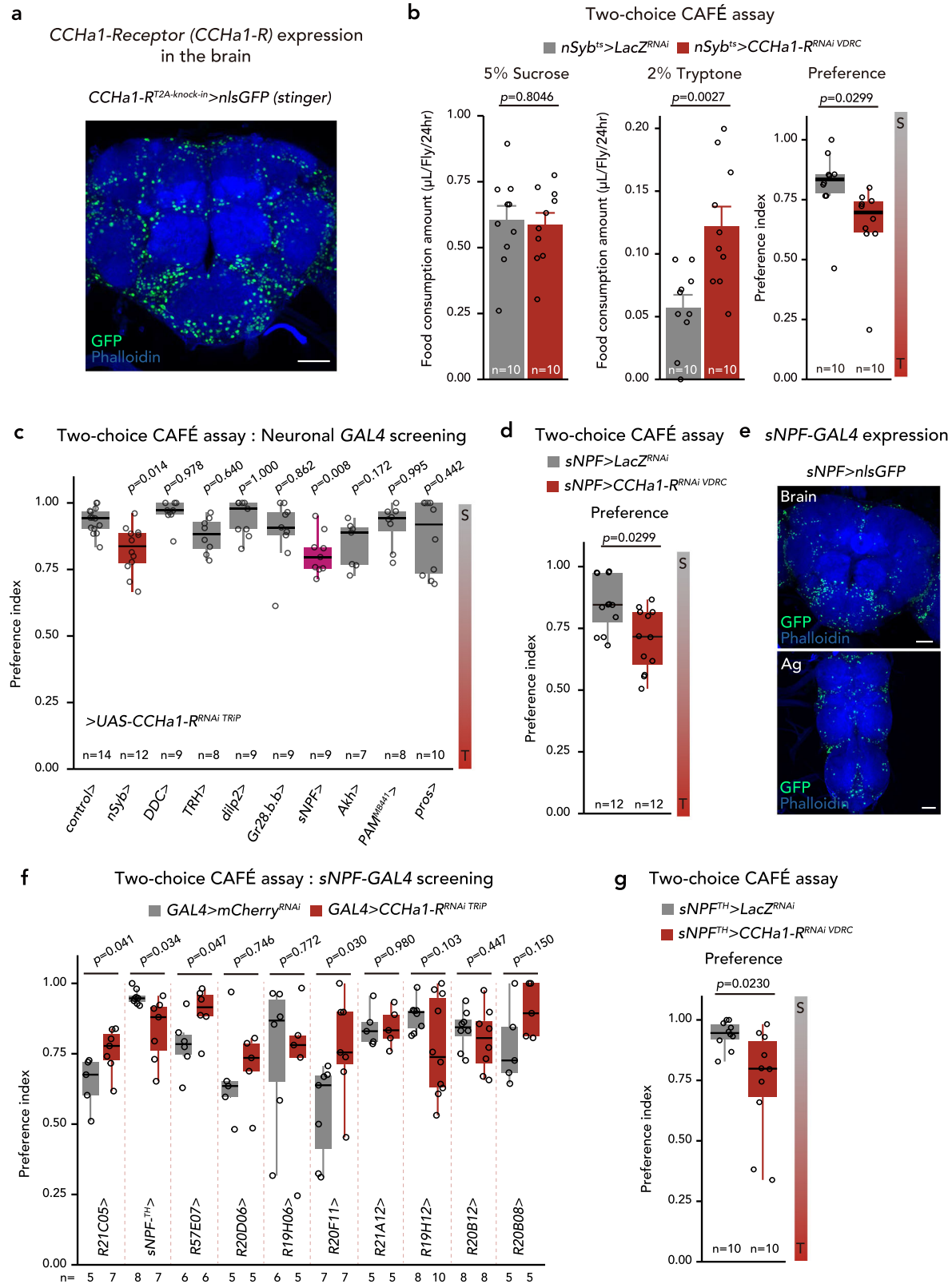

The next question to be addressed was whether CCHa1 secreted from the gut acts directly on enteric sNPF neurons. Therefore, we used the knock-in-Tango system, which enables us to investigate receptor signaling activity[33] (Fig. 4h). We employed *CCHa1-R-knock-in-Tango* with gut-specific *CCHa1* knockdown and found that loss of gut-derived CCHa1 reduced CCHa1-R signaling activity in enteric sNPF neurons (Fig. 4i, j). To further explore the CCHa1-R-sNPF pathway, we examined the effect of *CCHa1* overexpression in EECs. EEC-specific *CCHa1* overexpression shifted their preference toward sucrose in control (*sNPF* heterozygous mutant) genetic background, while the effect was diminished in *sNPF* null mutants (Fig. 4k, Supplementary Fig. 7a, b). These data support our idea that gut-derived CCHa1 suppresses protein feeding through enteric sNPF neurons.

Fig. 3 | CCHa1-R in sNPF neurons regulates feeding preference. **a** Immunostaining image of the brain from *CCHa1-R-T2A-knock-in-GAL4>stinger* flies expressing nuclear-localized GFP in the *CCHa1-R*-expressing cells. GFP (green) and phalloidin (blue) are shown. Scale bar, 50 μm. **b** Two-choice feeding experiment with CAFÉ assay. Consumption of sucrose (left), tryptone (centre), and preference (right) of control and neuronal *CCHa1-R* RNAi flies are shown. In the preference graph, S means sucrose, T means tryptone. **c** two-choice feeding experiment screening with the CAFÉ assay. Preferences between sucrose and tryptone of control (no GAL4) and several neurotransmitters, and neuropeptides expressing cell-specific *CCHa1-R* RNAi flies are shown. **d** Two-choice feeding experiment with the CAFÉ assay. Preferences between sucrose and tryptone of control and sNPF neurons-specific *CCHa1-R* RNAi flies are shown. **e** Immunostaining images of the brain (top) and abdominal ganglion (bottom: Ag) from *sNPF>stinger* flies expressing nuclear-localized GFP in the *sNPF* neurons. GFP (green) and phalloidin (blue) are shown. Scale bar, 50 μm. **f** Two-choice feeding experiment screening with CAFÉ assay. Preferences between sucrose and tryptone of control (*GAL4>mCherry RNAi*) and various *sNPF-GAL4*-driven *CCHa1-R* RNAi flies are shown. **g** Two-choice feeding experiment with CAFÉ assay. Preferences between sucrose and tryptone of control and enteric sNPF neuron-specific *CCHa1-R* RNAi flies are shown. In all graphs, numbers of samples assessed (*n*) are shown in the graphs. For all bar graphs, mean and SEM with all data points are shown. For box plots with dots, the median, 25th and 75th percentile lines are shown. Whiskers extend 1.5 times the interquartile range from the 25th and 75th percentiles. Statistics: two-tailed Student's *t* test (**b**, **d**, **f**, **g**), one-way ANOVA followed by Tukey's multiple comparisons test (**c**). *p* values are shown in the graphs.

Since *CCHa1* knockdown results in decreased mRNA expression of protein satiety factors *fit, dilp2*, and *dilp5*, we confirmed their expression in *sNPF* knockdown animals. As in *CCHa1* knockdown, *sNPF* knockdown decreased expression of *fit* and *dilp5*, but had no effect on *dilp2* expression (Supplementary Fig. 8a). These data suggest that in females, Fit is partially involved in CCHa1- and sNPF-mediated feeding control, but regulation of Dilp functions downstream of Fit may not be under the same control as the pathway. Consistent with the complexity of these downstream factors, mRNA expression of *CNMamide* (*CNMa*), a protein feeding facilitator produced in the gut[34], was upregulated by *CCHa1* knockdown and unaffected by *sNPF* knockdown (Supplementary Fig. 8b). Taken together with the *fit* and *dilps* expression data, various protein satiety factors appear to regulate feeding behavior downstream of CCHa1 and sNPF.

Mating significantly changes the feeding behavior of females. However, a shift in feeding preference to protein was observed in both mated *CCHa1* knockdown and *sNPF* knockdown animals (Supplementary Fig. 8c, d). These results suggest that CCHa1-sNPF feeding regulation works regardless of mating status.

Neuronal sNPF/sNPFR signaling is required for the control of feeding behavior

We next investigated how enteric sNPF neurons suppress protein feeding. Morphologically, enteric sNPF neurons project to the anterior part of the midgut and HCG neurons including sNPF-negative neurons (Fig. 5a, Supplementary Fig. 9a, b). The postsynaptic marker, DenMark[35], was localized in neurites in the gut (Fig. 5a). Furthermore, the presynaptic marker, Syt::GFP, was observed in neurites not only in the gut, but also on the HCG, implying that enteric sNPF neurons stimulate both tissues (Fig. 5a). Expression of the *sNPF receptor* (*sNPF-R*) was confirmed by *sNPF-R*$^{T2A\text{-}knock\text{-}in}$*-GAL4*-driven nuclear GFP signals. Nuclear GFP was observed in both sNPF-positive and -negative HCG neurons, the brain, and visceral muscle surrounding the anterior gut (Fig. 5b, Supplementary Fig. 9c). Knocking down *sNPF-R* in the nervous system resulted in a shift in feeding preference, whereas *sNPF-R* RNAi in muscle had no significant effect on the preference shift (Fig. 5c, Supplementary Fig. 9d, e). Moreover, neuronal *sNPF-R* knockdown promoted yeast intake, suggesting that sNPF-R in the nervous system is responsible for suppressing protein feeding (Fig. 5d).

To gain insight into neural circuits downstream of enteric sNPF neurons, we employed the Trans-Tango technique. Enteric sNPF neuron-driven Trans-Tango labeled neurons in the HCG by fluorescent reporter mtdTomato, suggesting that the neuronal pathway connects enteric sNPF neurons in the HCG with another set of HCG neurons (Fig. 5e). In contrast, the corpora cardiaca, labeled with AKH, was located in the vicinity of enteric sNPF neurons, no Trans-Tango signals were observed (Fig. 5e). Since *sNPF-R*$^{T2A\text{-}knock\text{-}in}$*-GAL4* was active in brain neurons (Supplementary Fig. 9c), we also investigated neurons labeled by Trans-Tango in the brain. We found that neurons in the superior lateral protocerebrum (SLP) and suboesophageal ganglion (SEG) were labeled as mtdTomato-positive downstream neurons (Supplementary Fig. 9f). However, similar signals were observed in controls without *GAL4* (Supplementary Fig. 9g), suggesting that those signals in the SLP and SEG constitute non-specific activation of Trans-Tango. Therefore, we focused on HCG neurons as a target of enteric sNPF neurons.

Enteric sNPF neurons send signals to sugar-sensing Gr43a neurons

There are two types of neurons in HCG, piezo neurons and Gr43a neurons[36,37]. Piezo neurons are activated by the mechanical stimulus of feeding, while Gr43a neurons are activated by sugar feeding[36,37]. Immunostaining analysis revealed that a subpopulation of piezo neurons was enteric sNPF neurons, whereas Gr43a neurons were distinct from sNPF neurons (Fig. 6a). To ascertain which neuronal population of HCG neurons is stimulated by enteric sNPF neurons, we knocked down *sNPF-R* in those HCG neurons. Knockdown of *sNPF-R* in piezo neurons did not increase protein and yeast intake in the feeding assay (Fig. 6b, Supplementary Fig. 10a, b). In contrast, knockdown of *sNPF-R* in Gr43a neurons led to enhanced protein preference and increased yeast autolysate intake, similar to knockdown of *sNPF* in enteric neurons (Fig. 6b, c, Supplementary Fig. 10c). Moreover, GFP Reconstitution Across Synaptic Partners (GRASP) analysis revealed that enteric sNPF neurons and HCG Gr43a neurons probably contact each other through synaptic connections (Fig. 6d). Importantly, the reduced sensitivity to sugar by knockdown of *Gr43a* in Gr43a neurons reduced yeast intake and increased sucrose intake (Fig. 6e). On the other hand, activation of Gr43a neurons by a temperature-dependent cation channel, TrpA1, increased yeast intake (Fig. 6f). These data suggest that enteric sNPF neurons regulate neuronal activity of sugar-sensing HCG Gr43a neurons to control the balance of sugar and yeast intake.

The gut-neuronal axis from gut-derived CCHa1 to HCG neurons influences the urea cycle and ammonium metabolism in HPD conditions

Given that loss of *CCHa1* or *sNPF* resulted in dysregulation of protein feeding, we expected that loss-of-function animals would substantially influence HPD-associated metabolism. To explore the role of CCHa1 and sNPF in adapting HPD, we performed metabolomic analysis using liquid chromatography-tandem mass spectrometry (LC-MS/MS) and compared metabolic profiles between SD and HPD conditions, as well as between control and EEC-specific *CCHa1* RNAi animals. In both genotypes, HPD led to significant metabolic changes, including increased levels of some amino acids (Fig. 7a, Supplementary Fig. 11a). HPD increased levels of glycine, methionine, and arginine, which are important in removing nitrogen from amino acids via the urea cycle and creatine-creatinine metabolic pathway (Fig. 7b). Pathway analysis also revealed that arginine biosynthesis, pyrimidine metabolism, and Ala/Asp/Glu metabolism are significantly affected, suggesting that amino acid metabolism and degradation are influenced by HPD feeding (Supplementary Fig. 11b).

In comparing control and *CCHa1* RNAi animals, we found a significant difference in levels of metabolites related to the urea cycle, a

https://doi.org/10.1038/s41467-024-55050-y

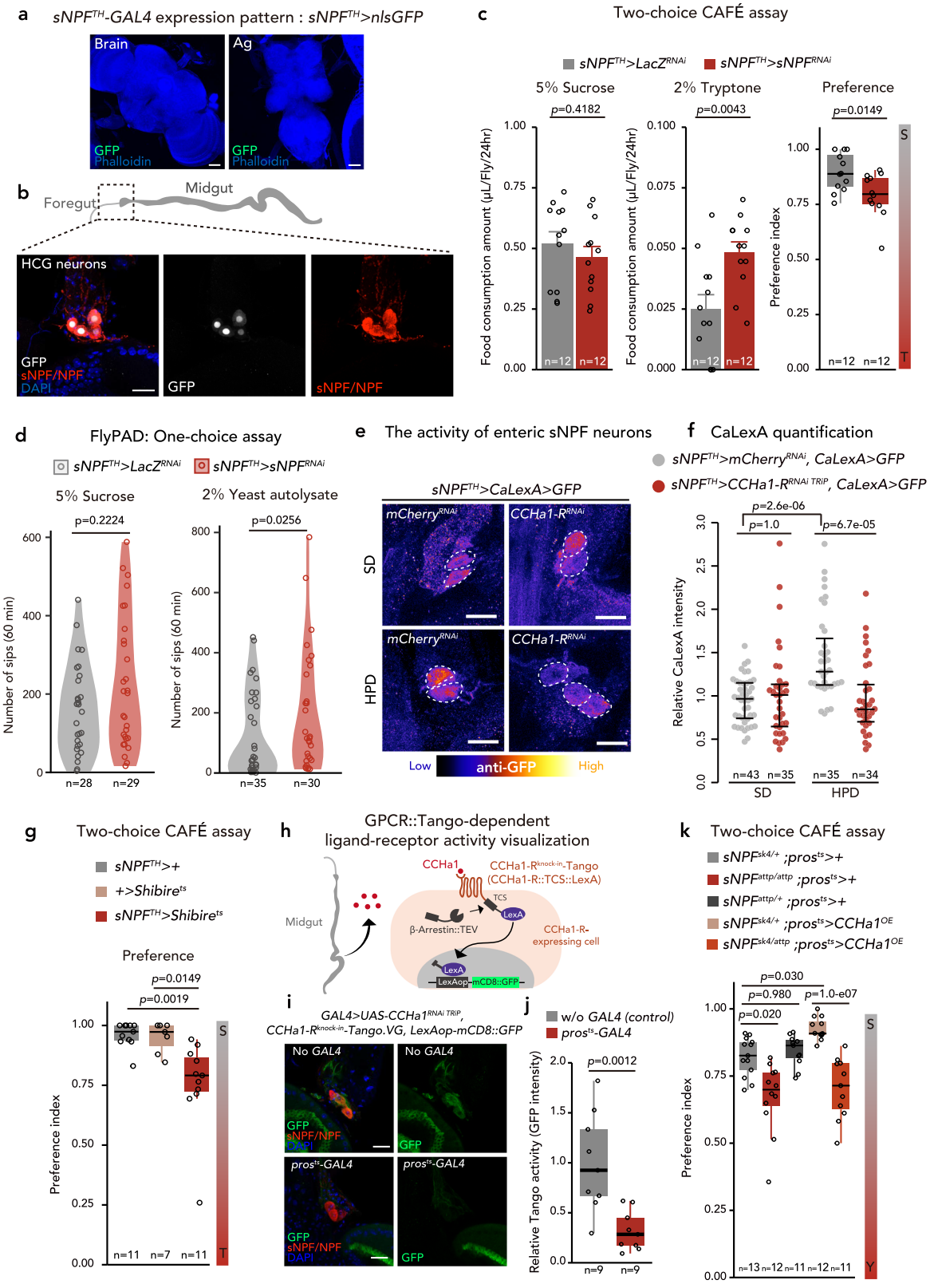

part of the arginine biosynthesis pathway, which detoxifies ammonium by incorporating it into ornithine and metabolizing it to citrulline[38]. Under HPD, *CCHa1* RNAi animals showed an increase in citrulline and an increasing trend for argininosuccinate, a metabolite of citrulline (Fig. 7b, Supplementary Fig. 12a–g). Moreover, several metabolites of the creatine metabolism pathway, which functions in conjunction with the urea cycle[39], also increased (Supplementary Fig. 12h–n).

Considering the accumulation of these intermediate products, we surmised that the urea cycle in gut-specific *CCHa1* knockdown animals would not be able to cope with amino acid metabolism. Therefore, we measured ammonium levels in whole-body samples to confirm whether *CCHa1* RNAi affects ammonium detoxication. As expected, HPD increased ammonium levels in both genotypes, but *CCHa1* RNAi animals exhibited a more significant increase in ammonium levels under

Fig. 4 | Enteric sNPF neurons control feeding behavior via sNPF. **a** Immunostaining images of the brain (left) and abdominal ganglion (right: Ag) from *sNPFTH>stinger* flies. GFP (green) and phalloidin (blue) are shown. Scale bar, 50 μm. **b** Illustration of the midgut (top) and immunostaining images of HCG neurons (bottom) from *sNPFTH>stinger* flies. GFP (white), sNPF/NPF (red), and DAPI (blue) are shown. Scale bar, 20 μm. **c** Two-choice feeding experiment with the CAFÉ assay. Consumption of sucrose (left), tryptone (centre), and preference (right) of control and enteric sNPF neuron-specific *sNPF* RNAi flies are shown. **d** Numbers of sips of sucrose (left) and yeast autolysate (right) of *sNPF* RNAi and control flies measured using the flyPAD system. **e** Pseudocolor images of enteric sNPF neurons from *sNPFTH>CaLexA > GFP* flies maintained on standard diet (SD) or 10% peptone-supplemented, high-protein diet (HPD). Fluorescence signals (GFP) are pseudo-coloured; high to low intensity is displayed as warm (yellow) to cold (blue) colors with a color scale. Scale bar, 20 μm. **f** Quantification of CaLexA-driven GFP intensity of enteric sNPF neurons. **g** Two-choice feeding experiment with CAFÉ assay. Preferences between sucrose and tryptone of controls and enteric sNPF neuron-inactive (*sNPFTH>shibire^{ts}*) flies are shown. **h** An illustration of GPCR::Tango system. Upon activation by ligand binding, β-Arrestin-TEV is recruited to GPCR and cleaves TCS, releasing LexA from the GPCR. **i** Immunostaining images of the HCG from control (without *GAL4* driver) or gut-specific *CCHa1* RNAi flies carrying *CCHa1-R-knock-in-Tango* and *LexAop-mCD8::GFP*. GFP (green), sNPF/NPF (red), and DAPI (blue) are shown. Scale bar, 20 μm. **j** Quantification of *CCHa1-R-knock-in-Tango* driven GFP intensity in the enteric sNPF neurons. **k** Two-choice feeding experiment with CAFÉ assay. The preference between sucrose and yeast autolysate is shown. Numbers of samples assessed (*n*) are shown in the graphs. For all bar graphs, means and SEMs with all data points are shown. For box plots with dots, the median, 25th and 75th percentile lines are shown. Whiskers extend 1.5 times the interquartile range from the 25th and 75th percentiles. All immunohistochemical experiments were repeated at least twice with similar results. Statistics: two-tailed Student's *t* test (**c**), two-sided Wilcoxon rank sum test (**d**, **j**), Wilcoxon rank sum test with Holm's correction (**f**), one-way ANOVA followed by Tukey's multiple comparisons test (**g**, **k**). *p* values are shown in the graphs.

HPD feeding (Fig. 7c). Moreover, knocking down *sNPF* or *CCHa1-R* in enteric sNPF neurons also increased ammonium levels (Fig. 7d, Supplementary Fig. 13a). Taken together, these findings suggest that the gut-neuronal axis by gut-derived CCHa1 and enteric sNPF neurons is essential to balance protein intake and urea cycle capacity.

Gut-derived CCHa1 and HCG neurons influence longevity in HPD conditions

Finally, we examined whether the gut-neuronal axis affects longevity in HPD conditions, as urea cycle disorders, leading to hyperammonemia, have a significant impact on survival in mammals[40]. Indeed, we found that gut-specific *CCHa1* RNAi animals exhibited a slightly reduced lifespan under SD compared to controls (Fig. 7e). In contrast, under HPD conditions, their lifespan was more significantly shortened (Fig. 7e). Moreover, enteric sNPF neuron-specific *sNPF* knockdown also shortened lifespan on HPD (Fig. 7f). Note that neither *CCHa1* knockdown nor *sNPF* knockdown affected lifespan on a sugar-only diet (Supplementary Fig. 13b, c). Taking the above results together, we revealed that the relay from gut-derived CCHa1 to HCG Gr43 neurons via enteric sNPF neurons suppresses excessive protein feeding, and as a result, excess ammonia production, which contributes to systemic adaptation to HPD (Fig. 7g).

Discussion

The ability to select appropriate foods according to nutritional status is essential in maintaining metabolic homeostasis. However, the mechanisms by which an organism senses and interprets its metabolic status to make food choices are not yet fully understood. This study demonstrates that a subset of EECs can detect protein content, followed by activation of a certain type of enteric neuron, leading to the transmission of protein intake signals to the CNS (Fig. 7g). More precisely, HPD stimulates the secretion of the gut hormone CCHa1, which influences sugar/protein intake and metabolic balance by stimulating sNPF enteric neurons. These enteric neurons, in turn, connect with downstream Gr43a sugar-sensing neurons in the HCG. Moreover, gut-derived CCHa1 and enteric sNPF ensure adult lifespan in HPD conditions, probably by suppressing the excessive accumulation of ammonia, at least in part. Taken together, we propose that gut-enteric neuron-brain communication is essential for optimal survival when flies consume a diet containing abnormal levels of protein (Fig. 7g).

Nutritional control in the activity of gut EECs

EECs release enteroendocrine hormones upon nutritional input[41,42]. Numerous dietary components, including sugars, amino acids, metals, and other small molecules, can activate EECs through their receptors and transporters[42–44]. For example, recent studies using *D. melanogaster* have highlighted the role of dietary carbohydrates in promoting the release of EEC hormones, such as Bursα and NPF, through solute ligand carrier 2 (SLC2) family sugar transporters and a gustatory receptor[11–13,15].

We found that the combination of excess Ala and Gly can activate CCHa1^{+} EECs. Receptors and transporters may be involved in sensing these amino acids. Still, specific receptors for Ala and Gly have yet to be identified in *D. melanogaster*, and the expression and function of amino acid transporters in the gut need to be better understood. Interestingly, since both Ala and Gly are essential for the activation of CCHa1^{+} EECs, EECs seem to read qualitative rather than quantitative information about amino acids. Future work should focus on Ala and Gly, as well as metabolites made from them, to determine how glycine and alanine activate EECs.

Gut-derived CCHa1 is highly responsive to an HPD and is essential to detoxify excess amino acids

Since extensive studies have established that a protein-rich diet significantly influences weight loss in various organisms[45,46], an HPD is considered a therapeutic intervention for obesity. Nonetheless, it has been suggested that an HPD may impair kidney function[47,48]. Our findings demonstrate that an HPD significantly affects the urea cycle metabolic pathway, which is critical for detoxifying amino acid-derived ammonia in *D. melanogaster*. Moreover, the loss of *CCHa1* in the gut apparently leads to altered levels of various intermediates of the urea cycle pathway and ammonia. A recent study has suggested that sleep deprivation remodels nitrogen metabolism, including ammonia, and exacerbates the toxicity of dietary nitrogen sources[49]. In addition, in light of our data and recent reports that gut-derived CCHa1 regulates sleep arousal[16], it is possible that the gut hormone, CCHa1, balances nitrogen intake and excretion by regulating feeding behavior and sleep in concert with the amount of dietary protein. Furthermore, dysfunction of CCHa1-sNPF signaling over a long period induces accumulation of ammonia, and its toxicity would be expected to shorten the lifespan of *D. melanogaster*. Thus, in *D. melanogaster*, gut-derived CCHa1 has a notable impact on nitrogen metabolism that might influence sleep and protein feeding. Of note, accumulation of excessive reactive oxygen species (ROS) in gut-associated sleep deprivation also shortens lifespan[50]. Since ammonia impairs mitochondrial function and promotes ROS production in human intestinal cells[51], it will be fascinating to see if gut-derived CCHa1 and nitrogen metabolism are involved in sleep loss-dependent ROS production.

Focusing on amino acid metabolism, the level of glycine, which affects the urea cycle and ammonia efflux (Fig. 7d), was elevated by HPD, suggesting that glycine may be actively synthesized from other amino acids and metabolites. We also found that creatinine, an amino acid derivative, is the metabolite most highly affected by HPD (30-fold increase). In mammals, creatinine is a metabolite of creatine, which is

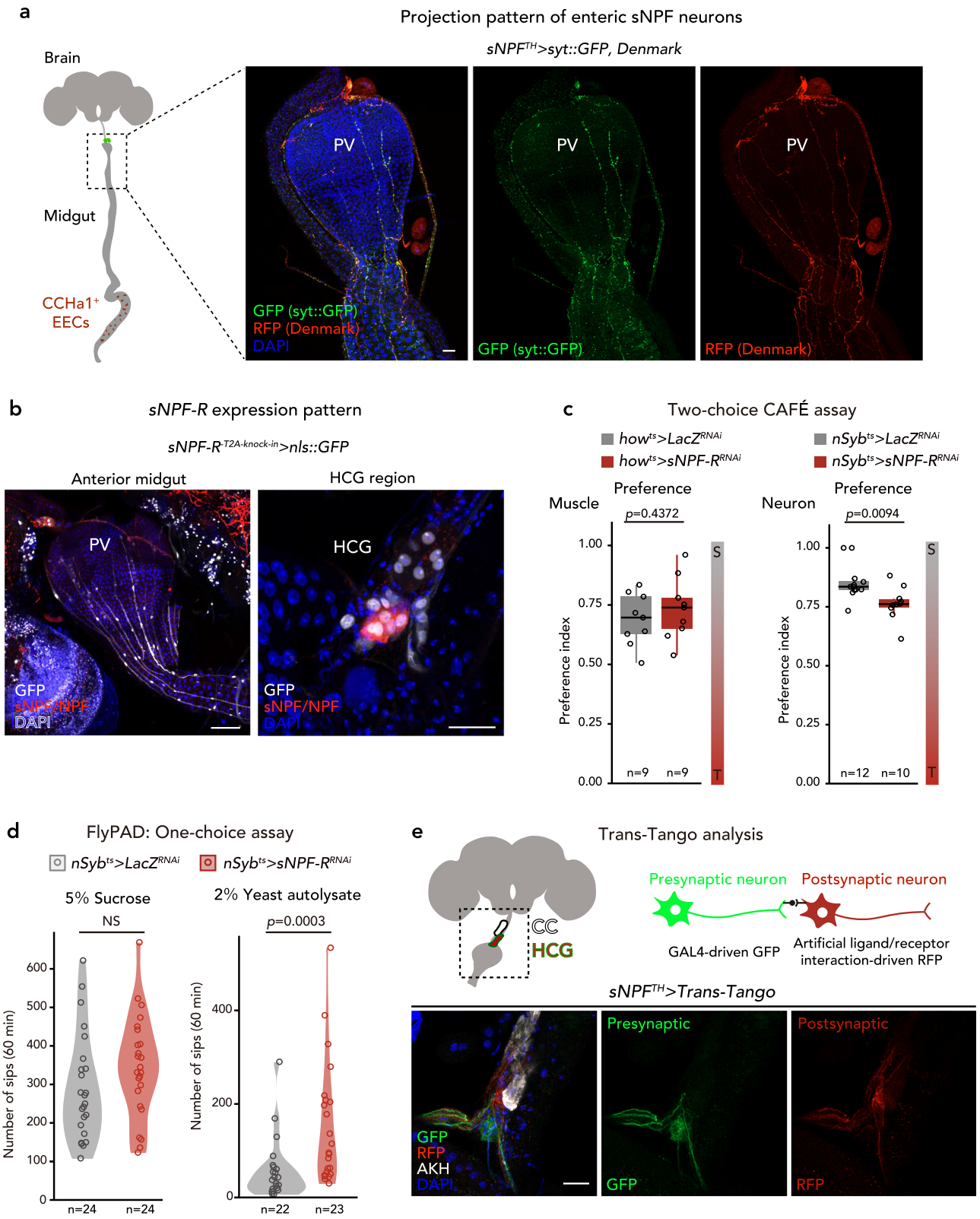

synthesized from glycine and arginine by the action of two enzymes: arginine:glycine amidinotransferase (AGAT) and guanidinoacetate methyltransferase (GAMT)[39]. While neither of these enzymes has yet been annotated and characterized in *D. melanogaster*, a similar pathway responsible for the conversion of amino acids to creatinine may prevent the accumulation of excess amino acids. We suppose that in *D. melanogaster*, uncharacterized enzymes with similar functions to AGAT and GAMT or microbiota in the gut may be involved in creatinine production in response to HPD. Disturbances in the balance of amino acid metabolism and accumulation of creatinine could also be an underlying cause of the shortened lifespan observed in response to HPD.

Feeding control by HCG neurons

Our data imply that there may be a complex interaction between the gut and neurons that regulate the production and excretion of

https://doi.org/10.1038/s41467-024-55050-y

Fig. 5 | Neuronal sNPF/sNPFR signaling regulates feeding behavior. **a** Immunostaining images of the anterior midgut from *sNPFTH>syt::GFP, Denmark* fly. GFP (green), RFP (red), and DAPI (blue) are shown. Scale bar, 20 μm. **b** Immunostaining images of the proventriculus (PV: left) and HCG (right) of *sNPF-R$^{T2A\text{-}knock\text{-}in}$>stinger* fly. GFP (white), sNPF/NPF (red), and DAPI (blue) are shown. Scale bar, 50 μm (left), 20 μm (right). **c** Two-choice feeding experiment with CAFÉ assay. Preferences between sucrose and tryptone of controls and muscle (*how^{ts} > sNPF-R^{RNAi}*)- or neuron (*nSyb^{ts} > sNPF-R^{RNAi}*)-specific *sNPF-R* RNAi flies are shown. S means sucrose, T means tryptone. **d** Numbers of sips on sucrose (left) and yeast autolysate (right) of *sNPF-R* RNAi and control flies measured using the flyPAD system. **e** Illustrations (top) and immunostaining images (bottom) of Trans-Tango experiment. Immunostaining images of the HCG of *sNPFTH>Trans-Tango* fly are shown with GFP (presynaptic neurons: green), RFP (postsynaptic neuron: red), AKH (corpora cardiaca: white), and DAPI (blue). Note that RFP signals were observed in HCG neurons, but not in the corpora cardiaca. Scale bar, 20 μm. Numbers of samples assessed (*n*) are shown in the graphs. For box plots with dots, the median, 25th and 75th percentile lines are shown. Whiskers extend 1.5 times the interquartile range from the 25th and 75th percentiles. All immunohistochemical experiments were repeated at least twice with similar results. Statistics: two-tailed Student's *t* test (**c**), two-sided Wilcoxon rank sum test (**d**). *p* values are shown in the graphs.

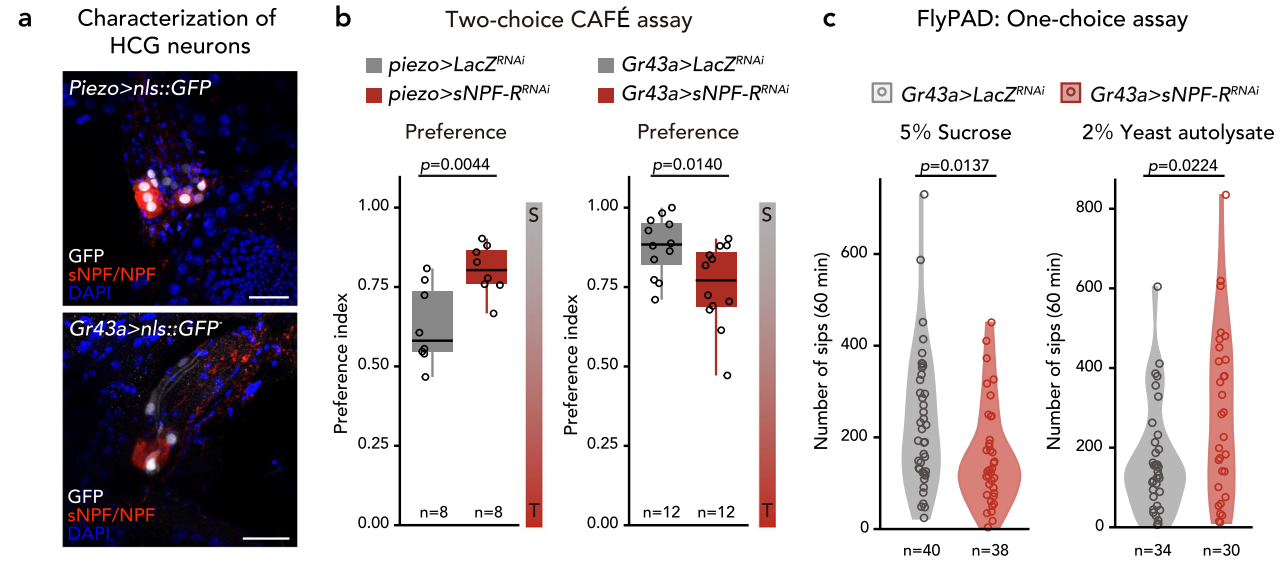

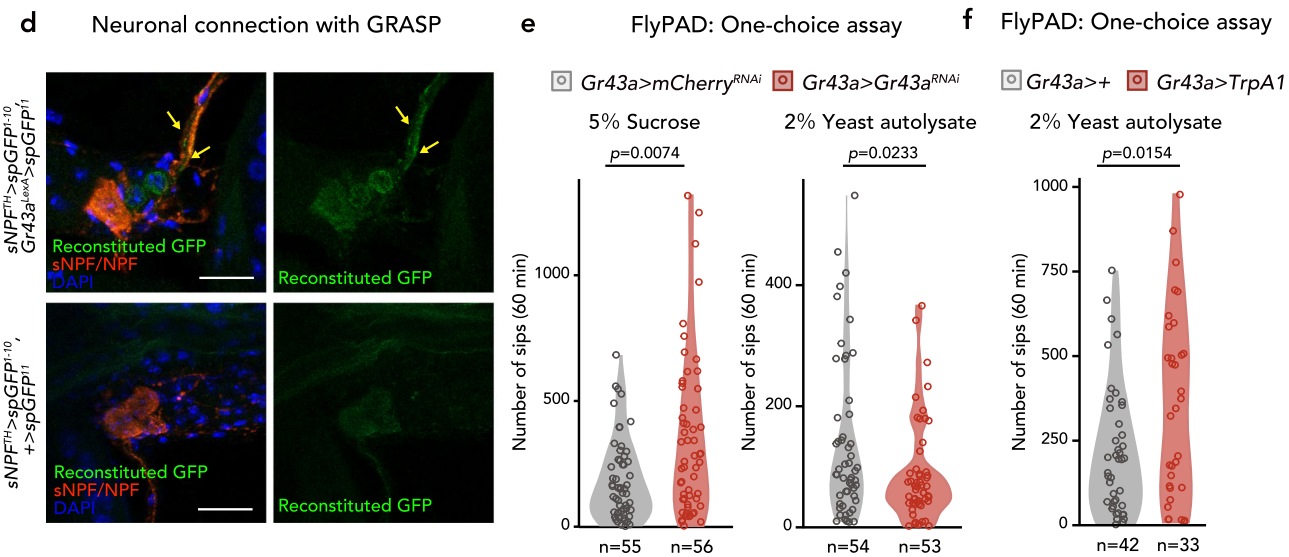

Fig. 6 | Enteric sNPF neurons send signals to sugar-sensing Gr43a neurons. **a** Immunostaining images of the HCG from *Piezo>stinger* (top), *Gr43a>stinger* (bottom) flies. GFP (white), sNPF/NPF(red), and DAPI (blue) are shown. Scale bar, 20 μm. **b** wo-choice feeding experiment with CAFÉ assay. Preferences between sucrose and tryptone of controls and piezo neurons (*Piezo > sNPF-R^{RNAi}*) or Gr43a neuron (*Gr43a > sNPF-R^{RNAi}*) specific *sNPF-R* RNAi flies are shown. S means sucrose, T means tryptone. **c** Numbers of sips of sucrose (left) and yeast autolysate (right) of *sNPF-R* RNAi and control flies measured using the flyPAD system. **d** Immunostaining images of the HCG of control (no *Gr43a-LexA*: bottom) and GRASP (with *Gr43a-LexA*: top) flies. Re-constituted GFP (without immunostaining: green), sNPF/NPF (red), and DAPI (blue) are shown. Yellow arrows indicate GRASP signals where nerves are in close proximity. Scale bar, 20 μm (right). **e** Numbers of sips of sucrose (left) and yeast autolysate (right) of *Gr43a* RNAi and control flies measured using the flyPAD system. **f** Numbers of sips of yeast autolysate upon activation of *Gr43a* neurons and control flies measured using the flyPAD system. Numbers of samples assessed (*n*) are shown in the graphs. For box plots with dots, the median, 25th and 75th percentile lines are shown. Whiskers extend 1.5 times the interquartile range from the 25th and 75th percentiles. All immunohistochemical experiments were repeated at least twice with similar results. Statistics: two-tailed Student's *t* test (**b**), two-sided Wilcoxon rank sum test (**c**, **e**, **f**). *p* values are shown in the graphs.

https://doi.org/10.1038/s41467-024-55050-y

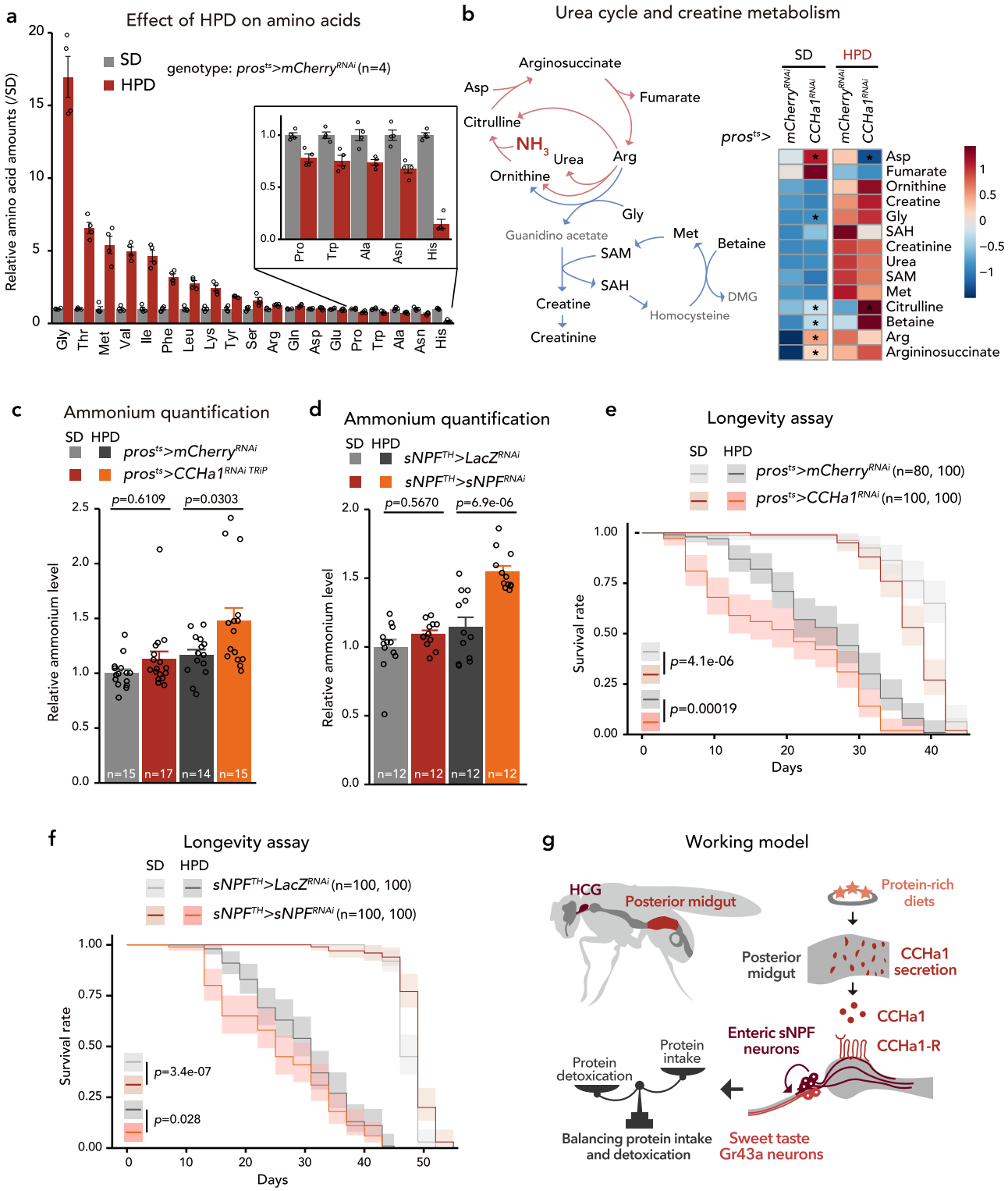

Fig. 7 | Gut-HCG neurons influence the urea cycle and ammonium metabolism. **a** Relative amounts of amino acids from whole body samples of *pros*^{ts}>*mCherry*^{RNAi} flies maintained on standard diet (SD) or high-protein diet (HPD). Values are normalized by SD. **b** An illustration of urea cycle and creatine metabolic pathway (left), and heatmaps of selected metabolites of control and gut-specific *CCHa1* RNAi flies maintained on SD or HPD. **c**, **d** Measurements of ammonium levels from whole body samples of control, gut-specific *CCHa1* RNAi flies (**c**), and enteric sNPF neurons specific *sNPF* RNAi flies (**d**). These flies were maintained on SD or HPD for 3 days before experiments. **e** Survival curves of control and gut-specific *CCHa1* RNAi flies maintained on SD or HPD. **f** Survival curves of control and enteric sNPF neuron-specific *sNPF* RNAi flies maintained on SD or HPD. **g** A model of this study. The numbers of samples assessed (*n*) are shown in the graphs. For all bar graphs, means and SEMs with all data points are shown. Survival curves show survival curve values and confidence intervals. Statistics: two-tailed Welch's *t* test (**b**), one-way ANOVA followed by Tukey's multiple comparisons test (**c**, **d**). Pairwise log-rank test (**e**, **f**), *p* values are shown in the graphs except for (**a**, **b**). *p* values and data of the (**b**) are shown in Supplementary Fig. 12.

proteolytic products to optimize their metabolism. We found that enteric sNPF neurons in the HCG are activated by gut-derived CCHa1 in response to HPD, suppressing protein feeding. Functions of sNPF neurons in the adult brain are well characterized in locomotion[52], feeding[53–55], and circadian behavior[56]. In contrast, although enteric sNPF neurons in the HCG have already been identified in *D. melanogaster* larvae[31,32], their functions in adults have not been reported. Our data provide evidence that enteric sNPF neurons have essential roles in food intake, and they provide an example of how neurons in peripheral tissues govern feeding behavior. sNPF is involved in feeding regulation in various insects, such as locusts[57], pea aphids[58], silkworms[59], and honeybees[60]. Especially, in mosquitos, Neuropeptide Y-like receptor LR7, a G protein-coupled receptor that can receive sNPF, regulates host-seeking behavior[61]. Therefore, it will be interesting to investigate whether sNPF neurons in the HCG or corresponding neuronal ganglia are present in other insects and whether they regulate feeding behavior in the same way as in *D. melanogaster*.

We also identified Gr43a neurons in the HCG as an essential downstream target of enteric sNPF neurons. Gr43a is a known fructose receptor that functions as a nutrient sensor in the brain and labial palps[37,62], but the function of Gr43a neurons in the HCG has not been characterized. Considering that HCG Gr43a neurons arborize their dendrites on the foregut, Gr43a neurons may directly sense fructose in the diet[36,37,63]. The involvement of Gr43a neurons implies that the interaction between proteins and sugars may be important in feeding preference, which should be investigated in the future. Such an interactive neuronal circuit may strengthen or weaken the manipulation of feeding motivation by CCHa1. We anticipate that the system would be necessary for making nutritional choices while allowing the organism to commit to protein levels that it can metabolize.

Since flies with *sNPF-R* RNAi in Gr43a neurons consumed more protein than controls, enteric sNPF neurons may modulate the sensitivity of fructose-sensing Gr43a neurons. Of note, knockdown of *Gr43a* increases and decreases intake of sugar and yeast, respectively, and activation by TrpA1 promotes yeast intake, supporting the idea that activation of Gr43a neurons promotes protein intake. Considering that sNPF neurons are negatively involved in promotion of protein intake, we should expect that sNFP-sNPF-R signaling inhibits Gr43 neuronal functions. It is noteworthy that sNPF-R couples with different types of G proteins, including the inhibitory Gi/o[55], raising the possibility that sNPF/sNPF-R signaling may suppress Gr43a neuronal activity. In the future, it will be intriguing to investigate how sNPF-sNPFR signaling and Gr43a signaling interact upon sugar and protein ingestion. Moreover, a future study should attempt to identify downstream targets of HCG Gr43a neurons.

In mammals, nutrient-responsive EECs secrete enteroendocrine hormones that are received by the vagal nerves whose dendrites are arborized on the gut[64,65]. Cell bodies of vagal nerves are located in the nucleus tractus solitarius (NTS) in the medulla of the brainstem, which synapses with the hypothalamus, containing the feeding centre[66]. It seems that the relationship between CCHa1^{+} EECs, enteric sNPF neurons, and HCG Gr43a neurons is partly analogous to the mammalian system in terms of the transmission of nutritional information from the gut to the feeding centre, which controls nutritional demands.

In recent years, the “protein-leverage hypothesis” has attracted attention as an interesting hypothesis for considering the relationship between protein intake and total food intake in mammals[67]. This hypothesis proposes that once a mammal has ingested a certain amount of protein, intake of additional food is suppressed. In mammals, molecular mechanisms for explaining the protein-leverage hypothesis are still largely unknown. On the other hand, the mechanism for suppressing protein intake, mediated by gut-derived CCHa1, the enteric sNPF neurons, and HCG Gr43a neurons discovered in this study is likely related to this hypothesis, even though it is a *Drosophila* system. While CCHa1 is not conserved in vertebrates, our study suggests the importance of intestinal hormones and the nervous system that receives them when testing the protein-leverage hypothesis in mammals. Comparing differences between the simpler *D. melanogaster* system and those of other model organisms, such as mice, will be a step toward understanding how nutrition-responsive behavioral and physiological responses have evolved among protostomes and deuterostomes.

Methods

Fly stocks and husbandry

Flies were raised on a standard fly food (8 g agar, 100 g glucose, 40 g dry yeast, 40 g corn flour, 4 mL propionic acid, and 3 mL 15% butyl p-hydroxybenzoate (in 100% ethanol) per litre) in 12/12 h light/dark conditions at 25 °C for 6 days before experiments. Genotypes that contained temperature-sensitive *tubulin-GAL80^{ts}* were raised at 20 °C for 3 days, after which they were incubated at 29 °C for 4 days to induce RNAi effects before experiments began.

The following transgenic and mutant stocks were used: *pros$^{\nu 1}$-GAL4* (a gift from Irene Miguel-Aliaga, MRC London), *R65D05-GAL4* (BDSC#39351), *nSyb-GAL4* (BDSC#51941), *Akh-GAL4* (BDSC#25684), *Ddc-GAL4* (BDSC#7010), *TRH-GAL4*[68] (a gift from Olga V. Alekseyenko, Harvard Medical School), *Gr28b.b-GAL4* (BDSC#57617), *sNPF-GAL4* (Kyoto Stock Center#113901), *PAM^{MB441}-GAL4* (BDSC#68251), *R21C05-GAL4* (BDSC#48933), *R57E07-GAL4* (BDSC#46382), *R20D06-GAL4* (BDSC#48892), *R19H06-GAL4* (BDSC#49840), *R20F11-GAL4* (BDSC#49852), *R21A12-GAL4* (BDSC#48925), *R19H12-GAL4* (BDSC#48869), *R20B12-GAL4* (BDSC#48880), *R20E08-GAL4* (BDSC#49851), *sNPFTH-GAL4* (BDSC#51991)[30], *dilp2-GAL4* (BDSC#37516), *how-GAL4* (BDSC#1767), *Gr43a-GAL4* (a gift from Chika Miyamoto and Hubert Amrein, Texas A&M University)[37], *Piezo-GAL4* (BDSC#59266), *tub-GAL80ts* (BDSC#7019), *R57C10-GAL80* (a gift from James W. Truman, University of Washington), *UAS-CCHa1* (This study), *UAS-stinger* (BDSC#84277), *UAS-myr::GFP* (BDSC#32198), *UAS-trans-Tango* (BDSC#77124), *CaLexA; UAS-mLexA-VP16-NFAT, LexAop-rCD2-GFP* (BDSC#66542), *UAS-syt::GFP, Denmark* (BDSC#33065), *GRASP; UAS-CD4-spGFP$^{1-10}$, LexAop-CD4-spGFP^{11}* (BDSC#58755), *UAS-GCaMP8f* (BDSC#92588), *UAS-TurboRFP* (Kyoto Stock Center#118640), *UAS-LacZ^{RNAi}* (a gift from Masayuki Miura, the University of Tokyo), *UAS-mCherry^{RNAi}* (BDSC#35785), *UAS-CCHa1^{RNAi}* (BDSC#57562), *UAS-CCHa1^{RNAi2}* (VDRC#104974), *UAS-CCHa1-R^{RNAi}* (BDSC#51168), *UAS-CCHa1-R^{RNAi2}* (VDRC#103055), *tub > FRT > GAL80 > FRT* (BDSC# 38879), *Otd-FLP* (a gift from Daisuke Yamamoto, National Institute of Information and Communications Technology, Japan)[69], *UAS-AstA^{RNAi}* (BDSC#25866), *UAS-AstC^{RNAi}* (BDSC#25868), *UAS-Tackykinin^{RNAi}* (BDSC#25800), *UAS-NPF^{RNAi}* (BDSC# 27237), *UAS-Bursα^{RNAi}* (BDSC#26719), *UAS-CCHa2^{RNAi}* (BDSC#57183), *UAS-Dh31^{RNAi}* (BDSC#41957), *UAS-Orcokinin^{RNAi}* (BDSC#61833), *UAS-sNPF^{RNAi}* (VDRC#330564), *UAS-sNPF-R^{RNAi}* (VDRC#330347), *UAS-Akh^{RNAi}* (BDSC#34960), *UAS-shibire^{ts}* (BDSC#66599), *UAS-TrpA1* (BDSC#26264), *sNPF^{sk4}*[70], *sNPF^{attp}* (BDSC#84574), *CCHa1$^{knock\text{-}in\text{-}T2A}$-GAL4*[71], *CCHa1-R$^{knock\text{-}in\text{-}T2A}$-GAL4*[71], *CCHa1-R$^{knock\text{-}in}$-TangoVG*[33,71], *tubP-β-Arrestin-TEV*[33], *13xLexAop2-mCD8::GFP*[33], *sNPF-R$^{knock\text{-}in\text{-}T2A}$-GAL4* (BDSC#84691).

w^{1118}, *UAS-LacZ^{RNAi}*, and *UAS-mCherry^{RNAi}* were used as the control. All data were obtained from females, except for Supplementary Fig. 1e, f and Supplementary Fig. 3f.

Genotypes that contained temperature-sensitive *tub-GAL80ts, TrpA1,* or *shibire^{ts}* were raised at 20 °C and kept adult for 3 days post-eclosion, after which they were incubated at 29 °C for 3-4 days before experiments began.

Food preparation

To prepare various diets, we added digested protein or a mixture of amino acids to a SD. 10% w/v Peptone (Thermo Fisher Scientific #211677) and tryptone (Thermo Fisher Scientific #211705) were used to

make HPDs. Throughout the manuscript, a 10% peptone-supplemented diet is referred to as HPD. Amino acid-supplemented diets were prepared by adding amino acids to a SD. A mix containing dissolved essential or NEAAs was prepared in advance, and materials equivalent to those in the SD were dissolved in the mix solution. The NEAA mix was divided into one acidic group (NEAA Mix1) and two other groups (NEAA Mix2-3). See Supplementary Data 1 for specific ingredients.

Generation of *UAS-CCHa1* line

Total RNA extracted from the heads of adult *Canton-S* flies was used to synthesize cDNA by reverse transcription (ReverTra Ace, Toyobo). The open reading frame of the *CCHa1* gene was amplified by PCR (Prime STAR Max DNA Polymerase, Takara Bio) on the cDNA using the following primers: forward primer (5′-CAAAATGTGGTACAGCAAGT GCAG-3′) and reverse primer (5′-CGGAATGTTCACTTCGTTAGCTC-3′). The PCR product was cloned into the pWALIUM10-moe vectors (RRID: DGRC_1470, *Drosophila* Genomics Resource Center) using the In-Fusion HD Cloning Kit (Takara Bio). The *UAS-CCHa1* construct was verified by sequencing and used for injection (BestGene). This construct was inserted into the ZH-86Fb site on the third chromosome using phiC31 site-directed integration.

Feeding assays

CAFÉ assays were conducted following a previously published protocol[72]. Four adult female flies were placed in separate tubes (21-mL tube, Sarstedt, 58.489) and two calibrated glass micropipettes (5 µL, Drummond Scientific Company, 2-000-001-90) filled with liquid medium (5% sucrose + 2.5% autolysed yeast extract) by capillary action were inserted through the sponge cap for 24 h at 29 °C and 70% relative humidity. Loss of media due to evaporation was controlled by subtracting readings from identical CAFÉ chambers lacking flies. Liquid media displacement readings were performed manually. The amount of liquid reduced in each capillary minus the amount of evaporation was defined as "consumption", and normalized by dividing by the number of flies examined, attaining µL/fly/h fed.

For two-choice CAFÉ assays, eight adult female flies were placed in separate tubes, and four calibrated glass micropipettes (5 µL, Drummond Scientific Company, 2-000-001-90) filled with liquid medium containing 5% sucrose, 2% autolysed yeast extract (Thermo Fisher Scientific #212750), 2% tryptone (Thermo Fisher Scientific #211705), or 10% NEAA solution (See Supplementary Data. 1) by capillary action were inserted through the sponge cap. Vials were inserted for 24 h at 29 °C and 70% relative humidity. Evaporation controls were set for both media. Consumption is calculated the same way as in the CAFÉ assay. For the sucrose vs. NEAA solution assay, flies were amino acid-deprived for 24 h on a 5% sucrose +1% agar diet prior to the CAFE assay.

FlyPAD assays were performed according to a previously described method[7]. A single fly starved in 1% agar for 16 h was placed in an arena with either 5% sucrose or 2.5% yeast autolysate solution, each mixed with 1% agar on a patch. In all experiments, flies were transferred to the flyPAD arena under light anesthesia and fed for 1 h at 29 °C and 70% relative humidity. The total number of sips per fly was calculated using previously described flyPAD algorithms[7].

Immunohistochemistry and fluorescence quantification

Fly tissues were dissected in 1× PBS and fixed in 4% paraformaldehyde in PBS for 30–60 min at room temperature (RT). Fixed samples were washed three times in PBS supplemented with 0.1% Triton X-100 (0.1% PBT). Samples were blocked in blocking solution (PBS with 0.1% Triton X-100 and 2% bovine serum albumin [BSA]) for 1 h at RT and then incubated with a primary antibody in the blocking solution at 4 °C overnight. Primary antibodies used in this study were chicken anti-GFP (1:4000, Abcam, #ab13970), rabbit anti-RFP (1:2000, Medical and Biological Laboratories, #PM005), mouse anti-Prospero (1:50; Developmental Studies Hybridoma Bank [DSHB]), mouse anti-CCHa1 (1:200, this study), guinea pig anti-sNPF/NPF[11] (1:2000; Note that this antibody recognizes both NPF and sNPF), mouse anti-AKH (1:200, this study). After washing, fluorophore (Alexa Fluor 488, 546, 555, or 633)-conjugated secondary antibodies (Thermo Fisher Scientific) were used at a 1:500 dilution, and samples were incubated for 2 h at RT in a blocking solution.

Midgut samples were dehydrated in a series of ethanol washes ranging from 10% to 90% on ice after fixation in 4% paraformaldehyde. Samples were kept in 90% ethanol for 20 min at RT followed by serial re-hydration, and subjected to the staining protocol described above.

Samples were visualized using a Zeiss LSM 700 confocal microscope or an LSM 800 confocal microscope. Images were processed using Fiji. Fluorescence intensity in confocal sections was measured with Fiji. We performed sum-intensity 3D projections to measure total fluorescent intensity across the object of interest (gut or neurons). For Tango reporter quantification, all enteric sNPF neurons were examined for each sample. To quantify immunostaining signal intensities with anti-sNPF antibody, cell bodies of all enteric sNPF neurons were examined for each sample.

Production of monoclonal antibodies

We produced mouse monoclonal antibodies against CCHa1 or AKH as described previously[73]. Briefly, a synthetic peptide of 13 amino acids with the sequence (N_3-SCLEYGHSCWGAH-$CONH_2$), which corresponds to a part of CCHa1, was conjugated to keyhole limpet hemocyanin (KLH) and an antigen emulsion was injected into BALB/c mice. Treated mice were euthanized 21 days after the injection, and lymphocytes were fused with SP2/0-Ag14 myeloma cells. After the cell fusion, culture supernatants were screened to confirm positive clones using a solid-phase enzyme-linked immunosorbent assay (ELISA). Anti-AKH antibody was made in a similar step using KLH-conjugated synthetic peptide with the sequence (NH_2-CQLTFSPDW-$CONH_2$).

CaLexA experiments

Collected virgin female flies were reared at 20 °C for three days before being used for experiments. Flies were then placed in vials (5–8 flies per vial) in various food conditions and kept at 29 °C for 3 days before dissection. Detailed information for food composition is listed in Supplementary Data 1. CaLexA-driven GFP intensity or CCHa1 protein intensity of each $CCHa1^+$ EEC in the posterior midgut was analyzed using the region of interest (ROI) of Fiji. Except for Supplementary Fig. 2c, the average GFP intensity in each gut is plotted. For Supplementary Fig. 2c, relative GFP intensity of all $CCHa1^+$ EECs is plotted. Cells indicating CaLexA-driven GFP intensity greater than 1.5-fold were defined as responders in Supplementary Fig. 2c.

Calcium imaging with GCaMP8f

To visualize intracellular Ca^{2+} levels in EECs with GCaMP8f, we used imaging methods described previously[74–76]. Midguts were dissected in Schneider's *Drosophila* medium (SDM) without supplementation with fetal bovine serum. Dissected tissues were attached to the bottom of the glass-bottomed dish (35 × 10 mm, IWAKI, #3910-035) with an insect pin (ϕ0.10 mm, Ento Sphinx Insect Pins) anchored by double-coated adhesive tape. Images were captured with a ×20 objective lens using a Zeiss LSM 800 confocal microscope and recorded every two seconds for two minutes. GCaMP8f fluorescence intensity in the EEC was then calculated for each time point in an ROI with Fiji. Fluctuations were visualized by normalizing the intensity at each time point to the average intensity throughout the recording. Time points with GCaMP8f intensity greater than 1.5-fold were defined as calcium peaks.

Quantitative reverse transcription PCR

To quantify changes in gene expression, midguts from 8 to 10 adult female flies, fly abdomen carcasses from 10 adult female flies, and

heads from 10 adult female flies were dissected for each sample. Total RNA was extracted using TRIzol (Thermo Fisher Scientific). cDNA was prepared with PrimeScript RT reagent Kit with gDNA Eraser (TAKARA). Quantitative reverse transcription PCR (RT-qPCR) was performed ABI PRISM 7500 or StepOnePlus Real-Time PCR system (Thermo Fisher Scientific) using TB Green Premix Ex TaqII (Takara Bio). Transcript levels of the target mRNA were normalized to *rp49* (*RpL32*) levels in the same samples. Primers used to measure transcript levels are represented in Supplementary Data. 2.

Knock in-Tango and Trans-Tango neuronal labeling

For knock in-Tango experiments, flies were reared at 20 °C until eclosion. Collected virgin female adult flies were kept at 29 °C for 6 days before dissection. Brain and gut complexes were dissected and subsequently processed for immunohistochemistry analysis as above. For the Trans-Tango experiment, adult flies were reared on SD at 25 °C for 6 days before dissection.

Lifespan assay

Virgin female files were reared for three days at standard density before being used for lifespan experiments. Collected flies were lightly anaesthetized with CO_2 and were sorted into vials (10 per vial) containing SD, HPD, or glucose diet (see Supplementary Data 1). Flies were kept at 29 °C during the experiment. Vials were exchanged every three days.

Ammonium quantification

Virgin female files were reared on a SD for three days after eclosion. Flies were transferred to a vial containing SD or HPD and raised an additional three days on that diet. Four flies were homogenized in 200 µL of PBS containing 0.1% Triton X-100 using a pellet pestle. They were immediately heat-inactivated at 80 °C for 10 min, and then cooled to RT. The supernatant was collected after centrifugation at 10,000 × *g* for 2 min at 4 °C. Ammonia was measured with colorimetric Ammonia Quantitation Kits (AAT Bioquest, no. 10059). Ten microliters of supernatant were mixed with 40 µL of Assay Buffer 1 on a 96-well plate and incubated at RT for 5 min. Then, 40 µL of Assay Buffer 2 was added to each well and incubated at RT for 30 min. Absorbance intensity was measured at 660 nm. The ammonium chloride standard, a kit component, was used as a standard and diluted with PBS containing 0.1% Triton X-100. Ammonia contents were normalized by protein amounts in supernatants measured with a BCA protein assay kit (Thermo Fisher Scientific #27225).

Metabolite extraction and a widely targeted metabolomics profiling

Widely targeted metabolomic analysis was performed as previously described[77,78]. In brief, frozen samples in 1.5-mL plastic tubes were homogenized in 300 µL cold methanol with a φ3 mm zirconia bead using a freeze crusher (Tokken Inc.) at 41.6 Hz for 2 min. Homogenates were mixed with 200 µL of methanol, 200 µL of H_2O, and 200 µL of $CHCl_3$ and vortexed for 20 min at RT. Samples were then centrifuged at 15,000 rpm (20,000 × *g*) for 15 min at 4 °C. Insoluble pellets were used to quantify total protein with a BCA protein assay kit (ThermoFisher Scientific). Supernatants were mixed with 350 µL of H_2O, vortexed for 10 min at RT, and centrifuged at 15,000 rpm for 15 min at 4 °C. Aqueous phases were collected and dried using a vacuum concentrator. Samples were re-dissolved in 2 mM ammonium bicarbonate (pH 8.0) containing 5% methanol and analyzed by LC-MS/MS.

Chromatographic separations in an Acquity UPLC H-Class System (Waters) were carried out under reverse-phase conditions using an ACQUITY UPLC HSS T3 column (100 mm × 2.1 mm, 1.8 µm particles, Waters) and under HILIC conditions using an ACQUITY UPLC BEH Amide column (100 mm × 2.1 mm, 1.7 µm particles, Waters). Ionized compounds were detected using a Xevo TQD triple quadrupole mass spectrometer coupled with an electrospray ionization source (Waters). Target metabolites were annotated based on the peaks of the standards for each metabolite. Peak areas of target metabolites were analyzed using MassLynx 4.1 software (Waters). Metabolite signals were normalized to total protein levels of corresponding samples after subtracting the values from the blank. *P* values were calculated using unpaired two-tailed Welch's *t*-tests in Microsoft Excel. Further statistical analyses, including PCA and pathway analysis, were performed in MetaboAnalyst 6.0 (https://www.metaboanalyst.ca/home.xhtml)[79]. Data were normalized to the median per sample. Metabolites that were statistically significant ($pros^{ts}$>*mCherry RNAi* vs $pros^{ts}$ > *CCHa1 RNAi*) were used for pathway analysis.

Statistics and reproducibility

All statistical analyses were carried out using "R." *p* values are provided in graphs, in comparisons with the appropriate control. All experiments were performed independently at least twice. All immunohistochemical experiments were repeated at least twice with similar results. In each experiment, we analyzed three or more specimens. The experiments were not randomized. The investigators were not blinded to allocation during experiments and outcome assessment. Although no statistical method was used to predetermine sample size, sample sizes were determined based on significance obtained from previous studies with similar experimental setups. Comparable sample sizes were used in each experiment. No data were excluded from the analyses.

Reporting summary

Further information on research design is available in the Nature Portfolio Reporting Summary linked to this article.

Data availability

Source data are provided with this paper.

References

1. Soultoukis, G. A. & Partridge, L. Dietary protein, metabolism, and aging. *Annu. Rev. Biochem.* **85**, 5–34 (2016).
2. Kosakamoto, H. et al. Sensing of the non-essential amino acid tyrosine governs the response to protein restriction in *Drosophila*. *Nat. Metab.* **4**, 944–959 (2022).
3. Jouandin, P. et al. Lysosomal cystine mobilization shapes the response of TORC1 and tissue growth to fasting. *Science* **375**, eabc4203 (2022).
4. Khan, M. S. et al. Protein appetite at the interface between nutrient sensing and physiological homeostasis. *Nutrients* **13**, 4103 (2021).
5. Simpson, S. J., Batley, R. & Raubenheimer, D. Geometric analysis of macronutrient intake in humans: the power of protein? *Appetite* **41**, 123–140 (2003).
6. Pesta, D. H. & Samuel, V. T. A high-protein diet for reducing body fat: mechanisms and possible caveats. *Nutr. Metab.* **11**, 53 (2014).
7. Itskov, P. M. et al. Automated monitoring and quantitative analysis of feeding behaviour in *Drosophila*. *Nat. Commun.* **5**, 4560 (2014).
8. Sun, J. et al. *Drosophila* FIT is a protein-specific satiety hormone essential for feeding control. *Nat. Commun.* **8**, 14161 (2017).
9. Kim, S. K., Tsao, D. D., Suh, G. S. B. & Miguel-Aliaga, I. Discovering signaling mechanisms governing metabolism and metabolic diseases with *Drosophila*. *Cell Metab.* **33**, 1279–1292 (2021).
10. Ribeiro, C. & Dickson, B. J. Sex peptide receptor and neuronal TOR/S6K signaling modulate nutrient balancing in *Drosophila*. *Curr. Biol.* **20**, 1000–1005 (2010).
11. Yoshinari, Y. et al. The sugar-responsive enteroendocrine neuropeptide F regulates lipid metabolism through glucagon-like and insulin-like hormones in *Drosophila melanogaster*. *Nat. Commun.* **12**, 4818 (2021).

12. Hoshino, R., Sano, H., Yoshinari, Y., Nishimura, T. & Niwa, R. Circulating fructose regulates a germline stem cell increase via gustatory receptor-mediated gut hormone secretion in mated *Drosophila*. *Sci. Adv.* **9**, eadd5551 (2023).
13. Malita, A. et al. A gut-derived hormone suppresses sugar appetite and regulates food choice in *Drosophila*. *Nat. Metab.* **4**, 1532–1550 (2022).
14. Kubrak, O. et al. The gut hormone allatostatin C/somatostatin regulates food intake and metabolic homeostasis under nutrient stress. *Nat. Commun.* **13**, 692 (2022).
15. Scopelliti, A. et al. A neuronal relay mediates a nutrient responsive gut/fat body axis regulating energy homeostasis in adult *Drosophila*. *Cell Metab.* **29**, 269–284.e10 (2019).
16. Titos, I. et al. A gut-secreted peptide suppresses arousability from sleep. *Cell* **186**, 1382–1397.e21 (2023).
17. Lin, H.-H. et al. A nutrient-specific gut hormone arbitrates between courtship and feeding. *Nature* **602**, 632–638 (2022).
18. Song, W. et al. Midgut-derived activin regulates glucagon-like action in the fat body and glycemic control. *Cell Metab.* **25**, 386–399 (2017).
19. Hadjieconomou, D. et al. Enteric neurons increase maternal food intake during reproduction. *Nature* **587**, 455–459 (2020).
20. Guo, X. et al. The cellular diversity and transcription factor code of *Drosophila* enteroendocrine cells. *Cell Rep.* **29**, 4172–4185.e5 (2019).
21. Fujiwara, Y. et al. The CCHamide1 neuropeptide expressed in the anterior dorsal neuron 1 conveys a circadian signal to the ventral lateral neurons in *Drosophila melanogaster*. *Front. Physiol.* **9**, 1276 (2018).
22. Asahina, K. Sex differences in drosophila behavior: qualitative and quantitative dimorphism. *Curr. Opin. Physiol.* **6**, 35–45 (2018).
23. Hudry, B. et al. Sex differences in intestinal carbohydrate metabolism promote food intake and sperm maturation. *Cell* **178**, 901–918.e16 (2019).
24. Wat, L. W. et al. A role for triglyceride lipase brummer in the regulation of sex differences in *Drosophila* fat storage and breakdown. *PLoS Biol.* **18**, e3000595 (2020).
25. Masuyama, K., Zhang, Y., Rao, Y. & Wang, J. W. Mapping neural circuits with activity-dependent nuclear import of a transcription factor. *J. Neurogenet.* **26**, 89–102 (2012).
26. Semaniuk, U. V. et al. Insulin-like peptides regulate feeding preference and metabolism in *Drosophila*. *Front. Physiol.* **9**, 1083 (2018).
27. Okamoto, N. & Nishimura, T. Signaling from glia and cholinergic neurons controls nutrient-dependent production of an insulin-like peptide for *Drosophila* body growth. *Dev. Cell* **35**, 295–310 (2015).
28. Sudhakar, S. R. et al. Insulin signalling elicits hunger-induced feeding in *Drosophila*. *Dev. Biol.* **459**, 87–99 (2020).
29. Li, H. et al. Fly Cell Atlas: A single-nucleus transcriptomic atlas of the adult fruit fly. *Science* **375**, eabk2432 (2022).
30. Asahina K. D. Neuropeptide-GAL4 constructs and insertions. *Flybase* http://flybase.org/reports/FBrf0222772.htm.
31. Carlsson, M. A., Enell, L. E. & Nässel, D. R. Distribution of short neuropeptide F and its receptor in neuronal circuits related to feeding in larval *Drosophila*. *Cell Tissue Res.* **353**, 511–523 (2013).
32. Veenstra, J. A. Peptidergic paracrine and endocrine cells in the midgut of the fruit fly maggot. *Cell Tissue Res.* **336**, 309–323 (2009).
33. Katow, H., Takahashi, T., Saito, K., Tanimoto, H. & Kondo, S. Tango knock-ins visualize endogenous activity of G protein-coupled receptors in *Drosophila*. *J. Neurogenet.* **33**, 44–51 (2019).
34. Kim, B. et al. Response of the microbiome–gut–brain axis in *Drosophila* to amino acid deficit. *Nature* **593**, 570–574 (2021).
35. Nicolaï, L. J. J. et al. Genetically encoded dendritic marker sheds light on neuronal connectivity in *Drosophila*. *Proc. Natl Acad. Sci. USA* **107**, 20553–20558 (2010).
36. Min, S. et al. Control of feeding by Piezo-mediated gut mechanosensation in *Drosophila*. *Elife* **10**, e63049 (2021).
37. Miyamoto, T., Slone, J., Song, X. & Amrein, H. A fructose receptor functions as a nutrient sensor in the *Drosophila* brain. *Cell* **151**, 1113–1125 (2012).
38. Matsumoto, S. et al. Urea cycle disorders-update. *J. Hum. Genet.* **64**, 833–847 (2019).
39. Wyss, M. & Kaddurah-Daouk, R. Creatine and creatinine metabolism. *Physiol. Rev.* **80**, 1107–1213 (2000).
40. Machado, M. C. C. & Pinheiro da Silva, F. Hyperammonemia due to urea cycle disorders: a potentially fatal condition in the intensive care setting. *J. Intensive Care Med.* **2**, 22 (2014).
41. Kaelberer, M. M. et al. A gut-brain neural circuit for nutrient sensory transduction. *Science* **361**, eaat5236 (2018).
42. Gribble, F. M. & Reimann, F. Function and mechanisms of enteroendocrine cells and gut hormones in metabolism. *Nat. Rev. Endocrinol.* **15**, 226–237 (2019).
43. Drucker, D. J. Mechanisms of action and therapeutic application of glucagon-like peptide-1. *Cell Metab.* **27**, 740–756 (2018).
44. Reimann, F., Tolhurst, G. & Gribble, F. M. G-protein-coupled receptors in intestinal chemosensation. *Cell Metab.* **15**, 421–431 (2012).
45. Moon, J. & Koh, G. Clinical evidence and mechanisms of high-protein diet-induced weight loss. *J. Obes. Metab. Syndr.* **29**, 166–173 (2020).
46. Song, T. et al. Dietary cysteine drives body fat loss via FMRFamide signaling in *Drosophila* and mouse. *Cell Res.* https://doi.org/10.1038/s41422-023-00800-8 (2023).
47. Knight, E. L., Stampfer, M. J., Hankinson, S. E., Spiegelman, D. & Curhan, G. C. The impact of protein intake on renal function decline in women with normal renal function or mild renal insufficiency. *Ann. Intern. Med.* **138**, 460–467 (2003).
48. Fouque, D. & Aparicio, M. Eleven reasons to control the protein intake of patients with chronic kidney disease. *Nat. Clin. Pract. Nephrol.* **3**, 383–392 (2007).
49. Bedont, J. L. et al. Chronic sleep loss sensitizes *Drosophila melanogaster* to nitrogen stress. *Curr. Biol.* **33**, 1613–1623.e5 (2023).
50. Vaccaro, A. et al. Sleep loss can cause death through accumulation of reactive oxygen species in the gut. *Cell* **181**, 1307–1328.e15 (2020).
51. Yokoo, K., Yamamoto, Y. & Suzuki, T. Ammonia impairs tight junction barriers by inducing mitochondrial dysfunction in Caco-2 cells. *FASEB J.* **35**, e21854 (2021).
52. Kahsai, L., Martin, J.-R. & Winther, A. M. E. Neuropeptides in the *Drosophila* central complex in modulation of locomotor behavior. *J. Exp. Biol.* **213**, 2256–2265 (2010).
53. Lee, K.-S., You, K.-H., Choo, J.-K., Han, Y.-M. & Yu, K. *Drosophila* short neuropeptide f regulates food intake and body size. *J. Biol. Chem.* **279**, 50781–50789 (2004).
54. Lee, K.-S. et al. *Drosophila* short neuropeptide F signalling regulates growth by ERK-mediated insulin signalling. *Nat. Cell Biol.* **10**, 468–475 (2008).
55. Oh, Y. et al. A glucose-sensing neuron pair regulates insulin and glucagon in Drosophila. *Nature* **574**, 559–564 (2019).
56. Johard, H. A. D. et al. Peptidergic clock neurons in *Drosophila*: ion transport peptide and short neuropeptide F in subsets of dorsal and ventral lateral neurons. *J. Comp. Neurol.* **516**, 59–73 (2009).
57. Dillen, S. et al. Functional characterization of the short neuropeptide F receptor in the desert locust, *Schistocerca gregaria*. *PLoS One* **8**, e53604 (2013).

58. Amir, M. B. et al. Short neuropeptide F and its receptor regulate feeding behavior in pea Aphid (*Acyrthosiphon pisum*). *Insects* **13**, 282 (2022).
59. Nagata, S. et al. Effects of starvation on brain short neuropeptide F-1, −2, and −3 levels and short neuropeptide F receptor expression levels of the silkworm, *Bombyx mori*. *Front. Endocrinol.* **3**, 3 (2012).
60. Bestea, L. et al. The short neuropeptide F regulates appetitive but not aversive responsiveness in a social insect. *iScience* **25**, 103619 (2022).
61. Duvall, L. B., Ramos-Espiritu, L., Barsoum, K. E., Glickman, J. F. & Vosshall, L. B. Small-molecule agonists of *Ae. aegypti* Neuropeptide Y receptor block mosquito biting. *Cell* **176**, 687–701.e5 (2019).
62. Fujii, S. et al. *Drosophila* sugar receptors in sweet taste perception, olfaction, and internal nutrient sensing. *Curr. Biol.* **25**, 621–627 (2015).
63. Musso, P.-Y., Junca, P. & Gordon, M. D. A neural circuit linking two sugar sensors regulates satiety-dependent fructose drive in *Drosophila*. *Sci. Adv.* **7**, eabj0186 (2021).
64. Tan, H.-E. et al. The gut-brain axis mediates sugar preference. *Nature* **580**, 511–516 (2020).
65. Li, M. et al. Gut-brain circuits for fat preference. *Nature* **610**, 722–730 (2022).
66. Baker, E. & Lui, F. Neuroanatomy, Vagal Nerve Nuclei. In *StatPearls* (StatPearls Publishing, Treasure Island (FL), 2022).
67. Raubenheimer, D. & Simpson, S. J. Protein leverage: theoretical foundations and ten points of clarification. *Obesity* **27**, 1225–1238 (2019).
68. Alekseyenko, O. V., Lee, C. & Kravitz, E. A. Targeted manipulation of serotonergic neurotransmission affects the escalation of aggression in adult male *Drosophila melanogaster*. *PLoS One* **5**, e10806 (2010).
69. Asahina, K. et al. Tachykinin-expressing neurons control male-specific aggressive arousal in *Drosophila*. *Cell* **156**, 221–235 (2014).
70. Ameku, T. et al. Midgut-derived neuropeptide F controls germline stem cell proliferation in a mating-dependent manner. *PLoS Biol.* **16**, e2005004 (2018).
71. Kondo, S. et al. Neurochemical organization of the *Drosophila* brain visualized by endogenously tagged neurotransmitter receptors. *Cell Rep.* **30**, 284–297.e5 (2020).
72. Ja, W. W. et al. Prandiology of *Drosophila* and the CAFE assay. *Proc. Natl Acad. Sci. USA* **104**, 8253–8256 (2007).
73. Kobayashi, T. et al. An improved iliac lymph node method for production of monoclonal antibodies. *Dev. Growth Differ.* **64**, 38–47 (2022).
74. Yoshinari, Y. et al. Neuronal octopamine signaling regulates mating-induced germline stem cell increase in female *Drosophila melanogaster*. *Elife* **9**, e57101 (2020).
75. Gao, J. et al. Dietary L-Glu sensing by enteroendocrine cells adjusts food intake via modulating gut PYY/NPF secretion. *Nat. Commun.* **15**, 3514 (2024).
76. Kurogi, Y. et al. Female reproductive dormancy in *Drosophila* is regulated by DH31-producing neurons projecting into the corpus allatum. *Development* **150**, dev201186 (2023).
77. Nishimura, T. Feedforward regulation of glucose metabolism by steroid hormones drives a developmental transition in *Drosophila*. *Curr. Biol.* **30**, 3624–3632.e5 (2020).
78. Yamada, T., Hironaka, K.-I., Habara, O., Morishita, Y. & Nishimura, T. A developmental checkpoint directs metabolic remodelling as a strategy against starvation in *Drosophila*. *Nat. Metab.* **2**, 1096–1112 (2020).
79. Pang, Z. et al. Using MetaboAnalyst 5.0 for LC-HRMS spectra processing, multi-omics integration and covariate adjustment of global metabolomics data. *Nat. Protoc.* **17**, 1735–1761 (2022).

Acknowledgements

We thank Olga V. Alekseyenko, Irene Miguel-Aliaga, Chika Miyamoto, Hubert Amrein, James W. Truman, Masayuki Miura, Daisuke Yamamoto, Hiroko Sano, Maki Katsura, the Bloomington Stock Center, the Kyoto Stock Center (DGRC), the National Institute of Genetics, the Vienna Drosophila Resource Center, and the Developmental Studies Hybridoma Bank for providing stocks and reagents. We are also grateful to Steve D. Aird for editing the manuscript. This work was supported by grants from KAKENHI (22K20649 to Y.Y., 19H03265 to T.Y., and 22H00414 to R.N.) and from Japan Agency for Medical Research and Development AMED-CREST (20gm1110001 to R.N.). This work was also partly supported by the Cooperative Research Project Program of Life Science Center for Survival Dynamics, Tsukuba Advanced Research Alliance (TARA Center), University of Tsukuba.

Author contributions

Y.Y., T.N., and R.N. designed the experiments. Y.Y. performed most of the experiments and analyzed data. T.N. performed metabolomic analysis. T.Y., S.K., and H.T. established some fly strains. T.K. and M.M. generated antibodies. T.N. and R.N. supervised the work. Y.Y., T.N., and R.N. wrote the manuscript.

Competing interests

The authors declare no competing interests.

Additional information

Supplementary information The online version contains supplementary material available at https://doi.org/10.1038/s41467-024-55050-y.

Correspondence and requests for materials should be addressed to Yuto Yoshinari, Takashi Nishimura or Ryusuke Niwa.

Peer review information *Nature Communications* thanks Julia Cordero, and the other, anonymous, reviewer(s) for their contribution to the peer review of this work. A peer review file is available.